High yield synthesis of nanostructures from layered titanium diboride and their hydrogelation

A Thesis Submitted

In the Partial Fulfilment of the Requirements

For the Degree of

MASTER OF TECHNOLOGY

By

Manis Kumar Lenka

To the

INDIAN INSTITUTE OF TECHNOLOGY GANDHINAGAR

June 2019

Certificate

It is certified that the work contained in the thesis titled **"High yield synthesis of nanostructures from layered titanium diboride and their hydrogelation"** by **Manis Kumar Lenka** (17210049), has been carried out under my supervision and that this work has not been submitted elsewhere for a degree.

Prof. Kabeer Jasuja

Assistant Professor

Indian Institute of Technology Gandhinagar

Ahmedabad – 382355, India

Acknowledgment

Firstly, I would like to thank Prof. Kabeer Jasuja for giving me a chance to work with his group. His constant guidance and motivation helped me a lot to evolve as a good researcher. Also, his character influenced me in the right way to shape my career, so I am very thankful to him. Then I would like to thank my semester evaluation committee member Prof. Chinmay Ghoroi for his valuable suggestions and motivation, which has helped me immensely during the research work.

Most importantly, I would like to give my gratitude to Asha Liza James for her constant help and motivation, which has helped me significantly in the research work and thanks for supporting me like an elder sister. Moreover, I would like to thank Harini Gunda for her selfless help in my research work. I would also like to thank Saroj Kumar Das for his motivation and suggestion. Also, I would like to thank Rohit Saraswat and Ramchandra Gawas for helping me to learn experiments at the initial period of my research.

I want to thank Dr. Manish D. Shinde (CMET Pune) for doing TEM/HRTEM of my samples and Dr. Sudip Deb (IITB) for his help in Laser Raman spectroscopy. Then, I would like to thank the central instrument facilities of IIT Gandhinagar for allowing me to do the sample analysis and I am thankful to all the TAs Komal Pandey, Poonam Pandey, Varsha Thambi, and Simranjit Singh for their timely help. Also, I would like to thank Prof. Sameer V. Dalvi for allowing me to use the zeta potential analyzer and thankful to Rupanjali Prasad for helping me in performing the analysis. I want to thank Ashutosh Jena for his help in capturing good images in the optical microscope. I want to thank Prof. Prachi Thareja for allowing me to do a rheological analysis of my samples. Also, at the same time, I would like to especially thank Abhijeet Ojha for helping me in the rheological analysis.

Last but not least; I want to thank my family members for their belief and support in every aspect of my life.

Abstract

Two-dimensional materials gained immense interest from a wide range of researchers across the globe due to their high surface area, lightweight, and specific properties like photocatalytic activities, high-temperature stability, superconductivity, and so on. To use these materials efficiently, researchers are trying to form different macrostructures like hydrogel, aerogel, nanocomposites, and so on. The hydrogel is on the upper hand in various applications due to its properties like easy surface modification, high surface reactivity, stability over high temperature, and translocation into cells. Here, we demonstrated a high-yield method of obtaining nanostructures (nanosheets and nanowools) from the colloidal dispersion that forms a hydrogel. We have observed for the first time a gel formation from the nanostructures derived from TiB_2. The obtained nanosheets possess higher lateral dimensions as compared to the size of their parent TiB_2 crystals. The samples have been analyzed through HRTEM, FESEM, and AFM to find a possible reason for the formation of large sheets. We found that these nanosheets are formed by following a non-classical crystallization pathway. Also, the possible mechanism for the gel formation was found by doing zeta potential analysis and by following a reduction pathway. Through the reduction pathway, it was found that the gel formation occurs through the chemical interaction of the borate groups, which is supported by FTIR analysis. The presence of larger sheets was also observed from the optical microscope and AFM. The Raman spectroscopy shows a peak at 700 cm^{-1}, which indicates the presence of boron honeycomb planes. The amplitude sweep, frequency sweep, and time sweeps unveil the higher value of storage modulus (G´) as compared to loss modulus (G´´) indicating the gel formation after just synthesis. It was observed that the optimum value of G´ is going up to 350 Pa after eight days of synthesis of the hydrogel. It would be interesting to use the hydrogel in the drug delivery and the powder form of nanostructures in air filtration near future.

Keywords: Two-dimensional materials, nanosheets, hydrogel, large sheets, non-classical crystallization, chemical interaction, borate groups, storage modulus, and loss modulus.

Table of Contents

List of Figures

List of Tables

Chapter 1: Introduction

1.1 Nanotechnology: Big Picture of the Small World

Nanotechnology is all about the study of the atoms, molecules, and other things that remain roughly in the range of 0.1-100 nm.[1] The nanotechnology was introduced to the world by the famous American physicist Richard Feynman through his lecture, "There is plenty of room at the bottom" in 1957. His lecture inspired many scientists to think about miniaturizing objects like storage devices, machinery, and so on, which could be made considerably smaller and more compact. To his surprise one year later an electrical graduate from Caltech made electric motors having size 1/64th inch cubed.[2] He just spent 2.5 months and used tools such as a toothpick and watchmaker's lathe. Along with this, many breakthroughs occur, and from them, one was the discovery of the microscopes (Scanning tunneling microscope and Atomic force microscope). These microscopes provided an unprecedented visualization of atoms and bonds, which laid us to the discovery of different nano-sized materials.

1.2 Background:

1.2.1 Nanomaterials:

Nanomaterials are those materials, which have at least one dimension limited to 100 nm. The nanomaterials are mainly classified into four types according to their size. They are 0D, 1D, 2D, and 3D nanomaterials.[3] The 0D nanomaterials have three nano-sized dimensions that include quantum dots, hollow-spheres, onions, and nano lenses. The 1D nanomaterials have two nano-sized dimensions, and another dimension is in microns; these include nanotubes, nanorods, nanowires, and nanoribbons. Whereas 2D materials have one nano-sized dimension, and the other two dimensions are in microns; these include nanosheets, nanodiscs, nanoplates, nanoprisms, and nanowalls. Similarly, 3D nanomaterials have three dimensions in nanometers to microns, which include nanoflowers, nanocones, nanoballs, nannocoils, and nanopillars. Table 1.1 shows the classification of nanomaterials.

Types of nanomaterials	Nanosize dimension	Examples
0D nanomaterials	3	Quantum dots, nano lenses, hollow spheres, onions
1D nanomaterials	2	Nanorods, nanowires, nanoribbons
2D nanomaterials	1	Nanosheets, nanoplates, nanodiscs, nanoprisms, nanowalls
3D nanomaterials	0	Nanoflowers, nanocoils, nanocones, nanoballs, nanopillars

Table 1. 1 Classification of nanomaterials

1.2.2 Two-Dimensional (2D) Nanomaterials:

Two-dimensional (2D) nanomaterials are those whose thickness is less than ten nm.[4] These materials are quite strong within each layer due to ionic and covalent intralayer forces.[5] The first 2D material is graphene, a single layer of graphite, which was isolated in 2004 by Professor Andre Geim and Professor Konstantin Novoselov.[6] In graphene, the intralayer force is covalent, which made the material very strong.

These 2D materials are generally derived from the layered materials. Layered materials are those in which each plane of atoms are held together by interplanar forces which are weaker than intraplanar binding forces.[7] Layered materials are classified as van der Waal bonded layered materials and ionic bonded layered materials.

1.2.2.1 2D nanomaterials derived from van der Waals based layered materials:

Graphene was the first 2D nanomaterial, which was derived from the van der Waals layered material (graphite). After graphene, there has been much research on the field of 2D nanomaterials derived from van der Waals based layered materials. From then, the family of 2D nanomaterials derived from the transition metal dichalcogenides (TMDs) has been highly explored. Several studies show that it is possible to get the 2D nanomaterials from the

transition metal dichalcogenides (TMDs have the stoichiometry of MX_2 where M is Ti, Nb, Hf, Zr, Ta, and X is S, Se, Te).[8–10] Coleman et al. have shown that the exfoliation of van der Waals based layered materials like MoS_2, WS_2, $MoSe_2$, $MoTe_2$, $TaSe_2$, $NbSe_2$, $NiTe_2$, BN, and Bi_2Te_3 in common solvents. They reported that the best suitable solvents for the exfoliation of TMDs (such as $MoSe_2$ and WS_2) are N-methyl-pyrrolidine (NMP) and isopropanol (IPA).[11] Liu et al. reported the large scale production of h-BN nanosheets by solid-state exfoliation of h-BN with ammonia borane by ball milling method.[12] Similarly, other families of van der Waals based layered materials such as vanadium oxide derivatives, and other chalcogenides like $BiTe_3$, Sb_2Te_3, and β-FeSe have been exfoliated into nanostructures. [13,14]

1.2.2.2 2D nanomaterials derived from ionic based layered materials:

The initial thought of exfoliation was based on the separation of weakly bonded layers in the parent material. After that, many researchers have reported that they have exfoliated the layered materials even with the strong electrostatic force of attraction (ionic bond). The first report came in 2006 by Nakano et al., where they have exfoliated $CaSi_2$. Here, they have reduced the ionic bonding by doping with magnesium.[15] Similarly, Bianco et al. have shown the exfoliation of the germanium layers from the $CaGe_2$ and later shown the formation of hydrogen-terminated germanium layers (germanane) through topochemical deintercalation of CaGe2.[16]

1.2.3 Colloidal dispersion of 2D nanomaterials:

Nanomaterials in colloidal dispersion form have gained much interest for their potential applications as they provide easy access to surface modification, high reactivity on the surface, stability at high temperature, and translocation into cells.[17,18,19] Some of these applications depend on whether these nanomaterials are agglomerating or not. Nanomaterials/Nanoparticle agglomeration results due to the electrostatic forces of attraction. Particles with zero charges induce the agglomeration, which results in massive particles, and they settle due to the gravitational forces. If the particles are carrying some electric charges, then they repel each other and try to disperse in the solution. In this case, the colloidal dispersion is said to be stable.[20] Sometimes the stable colloidal dispersion of nanoparticles

forms a gel (three-dimensional networks that absorb solvents and swell to a limited degree without dissolution[21]).

1.2.4 Hydrogel: 2D nanomaterials dispersion

Hydrogels are known as hydrophilic gels in which the crosslinked networks extensively swelled with water.[22] When the hydrogels have the crosslinked networks consist of nanomaterials having sizes in the range of 10 nm – 1000 nm, then this is known as nanohydrogels.[23] The ability of the hydrogel to absorb water comes from the functional groups or crosslinkers attached to the networks, and their resistance to dissolution depends on the crosslinks between the network chain.[24] If the crosslink networks are fragile, then the gel will dissolve in water. Figure 1.1 showing the preparation method of the hydrogel. From this figure, we can see that the colloidal dispersion of nanoparticles in water resulted in hydrogel after some time. The water gets trapped in the networks between the nanoparticles and the crosslinker.

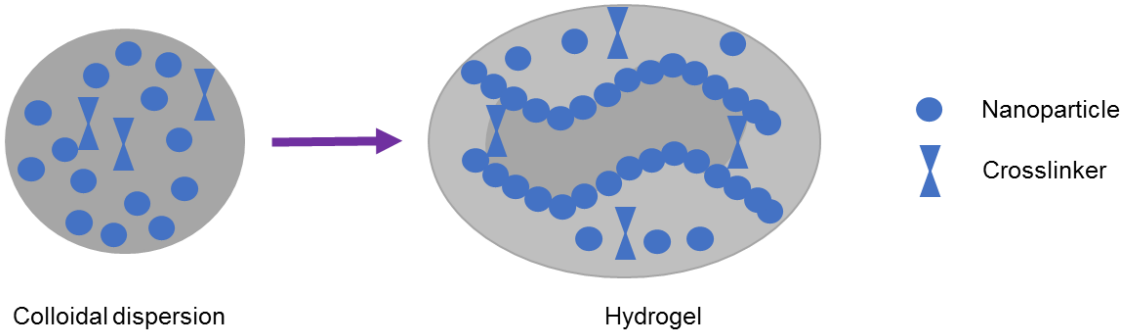

Figure 1. 1 hydrogel preparation showing the water gets trapped inside the crosslinking

1.3 Review on Group's work on nanoscaling metal diborides:

Our group is working on the synthesis and application of boron nanomaterials. The reason for synthesizing boron nanomaterials is due to its excellent properties like high melting point, high Young's modulus, high hardness in crystalline form, good electrical conductivity at high temperature, and inert with most chemicals.[25] So our thought process is to enable its quasi-planar 2D honeycomb lattice, which is expected to host a range of rich properties. We are using layered metal diborides as a parent material for synthesizing boron analogs of graphene.

1.3.1 Layered Metal diborides(MB_2 type):

A decent crystal structure is possessed by the metal diborides where the metal atoms are sandwiched between the alternative honeycomb layers of boron.[26] They have a general chemical formula of MB_2, where "M" is a metal (Mg, Al, Ti, Cr, Zr, Ta), and "B" is boron. From figure 1.2, we can see that each metal atom is intercalated to twelve boron atoms out of planes and six neighbor metal atoms in the same plane.

The bondings in layered metal diborides have the characteristic of ionic, covalent, and metallic. The in-plane boron atoms (B-B) is bonded with covalent bonds, whereas the in-plane metal atoms (M-M) are bonded with metallic bonds. The out-of-plane bond between the metal atom and the boron atom (M-B) is ionic. Also, the partial interaction of the p-electrons of the boron with d-electrons of metal atoms imparts covalent characteristics to the M-B bonds, thus resulting in a complex bonding between the metal and boron atoms.[27]

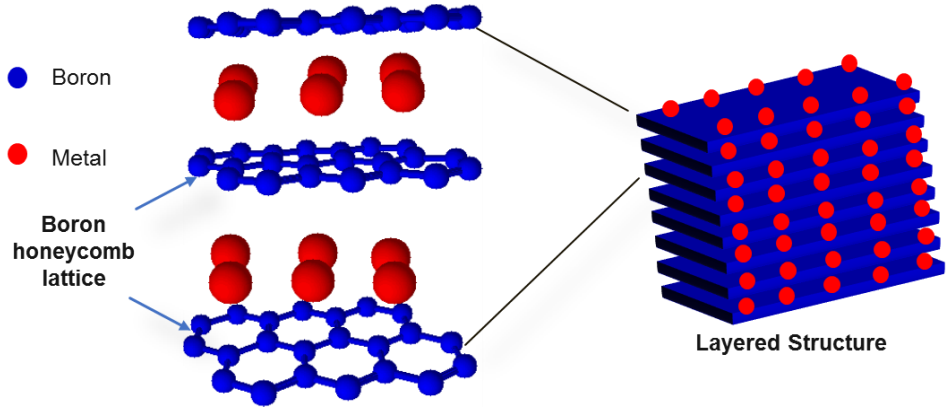

Figure 1. 2 Crystal structure of layered metal diborides showing metal atoms sandwiched between boron honeycomb planes.

1.3.2 Work Review:

S K Das et al. have exfoliated magnesium diboride for the first time. They showed that ultrasonication of magnesium diboride in water results in exfoliation of few-layer-thick Mg deficient hydroxyl functionalized boron-based nanosheets. They also reveal that the stability of these chemically modified sheets comes from the hydroxyl groups. These nanosheets exhibit a minimal absorption coefficient of 2.9 ml mg^{-1} cm^{-1} compared to graphene. [28]

A L James et al. have reported that it is possible to exfoliate metal borides like magnesium diboride and aluminum diboride in aqueous solution by using a chelating agent. Here they have extracted the metal atoms in between the boron planes by targeting these through a chelating agent. Also, they have found that these nanosheets are heavily decorated with functional groups like hydride and oxy-functional groups. [29]

H Gunda et al. demonstrated a simple and high yield (~92 %) method to obtain diverse morphologies of boron-based nanostructures from MgB_2. Here, they have obtained the boron-based nanostructures through a non-classical crystallization process. They have found that MgB_2 crystals undergo dissolution in water under ambient conditions, which result in prenucleation clusters that upon aging undergo non-classical crystallization preferentially growing in the lateral dimensions. They also observed the presence of hydride and oxy-functional groups on the surface of the sheets, which result in an overall negative charge of those sheets. [30]

S K Das et al. have found a chemical method to nanoscale MgB_2 where they have treated MgB_2 with acid followed by intercalation with organoammonium ions that swells the crystals and partly delaminates to form nano accordions, which was then sonicated in water to get nanosheets. They have found that these nanostructures are Mg deficient and functionalized with oxy-functional groups. They have also shown the use of this nanostructure as flame retardant nanofillers. They have found that these nanostructures have extraordinary flame retardant properties as compared to graphene and its analogs.[31]

A L James et al. have shown that magnesium diboride nanosheets obtained by exfoliation bear ability to promote the chemical reduction of quinone-based materials. These nanosheets also reduce gold salts into ultrasmall gold nanoparticles and graphene oxides into reduced graphene oxides. Also, they have found out that the metal nanoparticle-nanosheet hybrids have excellent electrocatalytic activity towards for hydrogen evolution reaction.[32]

R Saraswat et al. have shown high-yield chemical exfoliation of magnesium diboride. Here they have used organic chelating agents to synthesize boron-based nanosheets. They have chosen

the chelants, which have a greater affinity towards magnesium atoms such that the chelant can efficiently extract the interlayer Mg atoms from MgB_2 by leaving boron planes in water.[33]

1.4 Layered titanium diboride: as a prospective parent material:

Layered titanium diboride (TiB_2) is a cationic layered material in which titanium is a cation and boron is an anion. Here titanium ions are sandwiched between the boron honeycomb planes, that is why it is a cationic layered material. TiB_2 has ionic, covalent, and metallic bonding, and hence, it is a strong material.[34] It has attained much attention due to its exceptional properties like high hardness, high elastic modulus, high abrasion resistance, good electrical conductivity, and high melting points.[35,36] So it is widely used in the fields of cutting tools, electrodes, armors and structural materials.[37,38,39]

1.5 Research Problem and Questions:

The exfoliation of layered materials has resulted in several 2D materials. Among them, graphene is the most popular one due to its excellent properties, which comes from its carbon honeycomb planes. Inspired by the this we thought of taking this research to another level by accessing boron honeycomb planes from layered metal diborides. TiB_2 is chosen as the parent layered metal diboride due to its excellent properties, which is described above. The thought behind selecting TiB_2 is getting the access of boron honeycomb planes so that we can harness its properties to its full potential.

Recently, John et al. have shown the exfoliation of TiB_2 by ultrasonication in water to yield TiB_2 nanosheets. They were able to achieve only ~13% yield, which is quite less.[40] So our thought process was to get access to these boron honeycomb planes in titanium diboride with high yield. It is assumed that by applying chemical exfoliation method, we can get nanosheets with high yield as mechanical methods would not be that much effective for high yield due to its strong bonding between Ti and B. So, we aim to investigate the chemical exfoliation of TiB_2. It is found from the literature that titanium diboride is chemically inert with most chemicals.[41] But, we found an unexpected reaction of titanium diboride with hydrogen peroxide. We

observed that the titanium diboride upon reacting with a suitable concentration of hydrogen peroxide results in hydrogel formation. Thus, we posed three crucial questions:

(Q.1) As titanium diboride upon reaction with hydrogen peroxide forms a hydrogel with time, so the first question we posed was: What is in the dispersed phase of the hydrogel? Have we exfoliated the titanium diboride using hydrogen peroxide? If we have exfoliated the titanium diboride, then the dispersed phase of the hydrogel should contain nanosheets.

(Q.2) As the hydrogel was forming, so the second question that we posed was: how the hydrogel is forming upon simple mixing of titanium diboride with hydrogen peroxide?

(Q.3) If the gel is forming, so the third question that we posed was: what are the rheological properties of this hydrogel? Is this boron-based hydrogel have higher storage modulus than graphene oxide gels?

1.6 Organization of the thesis:

In **Chapter 1**, we have presented the background knowledge on nanomaterials, colloidal dispersion of nanomaterials, hydrogel, layered metal borides. Here we have given the first set of observation that we have made upon a simple reaction between titanium diboride and hydrogen peroxide.

In **Chapter 2**, we have demonstrated how we observed hydrogel formation. Also, we have discussed that the same recipe with time, did not result in the gel formation after the same days. Then how we change the concentration of reactants to get the gel formation again. Also, we have discussed the modification in the process of formation of the hydrogel. Here, we have found the presence of nanostructures with a high yield. Then we have demonstrated the difference between the different samples (obtained by varying the concentration of reactants) through different characterization like FESEM, FTIR, and XRD.

In **Chapter 3,** Here we have carried out time-dependent studies through TEM/HRTEM of the samples to find out what is happening inside the gel. Also, we have demonstrated how the zeta potential studies and reduction process were carried out to find out the mechanism of the gel

formation. In this chapter, we have analyzed the results from different characterization techniques like an optical microscope, Atomic force microscope, and TGA-DSC.

In **Chapter 4,** Here, we have discussed the properties of the hydrogels at different times, which was obtained by varying the reactant concentration through rheometer. Also, we have demonstrated whether the morphology of the dispersed phase is related to the gel formation or not. In **Chapter 5,** we have concluded all the essential results and mentioned about future work.

Chapter 2: Recipe of Hydrogelation

2.1 Introduction:

We have found the gel formation from the layered metal diborides upon simple mixing of layered titanium diboride crystals with hydrogen peroxide and water. Then we observe the condition of the gel formation and the parameters, which affect gel formation. Then we discuss the optimization of the parameter that is reaction time, which leads to a minimal amount of unreacted titanium diborides after the reaction. Also, we discuss different experiments that we performed by varying the ratio of the titanium diboride and hydrogen peroxide and optimize the same to get the gelation at a faster rate. Tyndall beam effect is used to test for the presence of colloidal dispersion. The FESEFM analysis is used to see the morphology of the dispersed phases after lyophilization of the hydrogel and is found to be nanosheets. The functional groups attached to these sheets are found to be from the FTIR analysis. Also, we discuss the study of the samples at different ratio of reactants and at a different reaction time and observe it under FESEM, FTIR, and XRD to see the difference in each sample.

2.1 Gel formation- An unexpected observation:

Our main aim was to get a high yield of nanosheets after exfoliation. That's why we followed a chemical exfoliation approach as mechanical exfoliation will need so much energy to break the Ti-B bonds. We chose hydrogen peroxide as chemicals as it has high reactivity with most materials. First, we added titanium diboride in the water; this resulted in a dark color suspension. To this suspension, hydrogen peroxide was added, which resulted in a yellow color solution with time. When this solution kept for some days, then an unexpected observation occurred. After five days, it is found to form a gel. This is the first time that we observe gel from the metal diborides.

2.1.1 Sample Preparation:

10ml of hydrogen peroxide (SD Fine Chem Limited, 30% (w/w)) was added to the suspension of 300 mg of titanium diboride (Sigma Aldrich, particle size < 10 µm and density= 4.52 g/ml) and 100ml of deionized water (Millipore Ultrapure Type I, Specific resistivity= 18.2 MΩ.cm). The

solution was subjected to magnetic stirring for 2 hours with a speed of 250 rpm. Then it was kept for 24 hours of settling, which is then followed by centrifugation.

Centrifugation:

The dark yellowish colored sample obtained after stirring was subjected to centrifugation (Thermo Fisher Scientific's Sorvall Legend X1R Centrifuge) at a speed of 8000 rpm for 15mins, at 20^{o}C. The supernatant was collected, which is yellow. The Tyndall effect test showed the presence of dispersed phases. The supernatant was kept for four days at room temperature in a closed glass bottle, and then it was observed to form a gel. Figure 2.1 showing the schematic of gel formation.

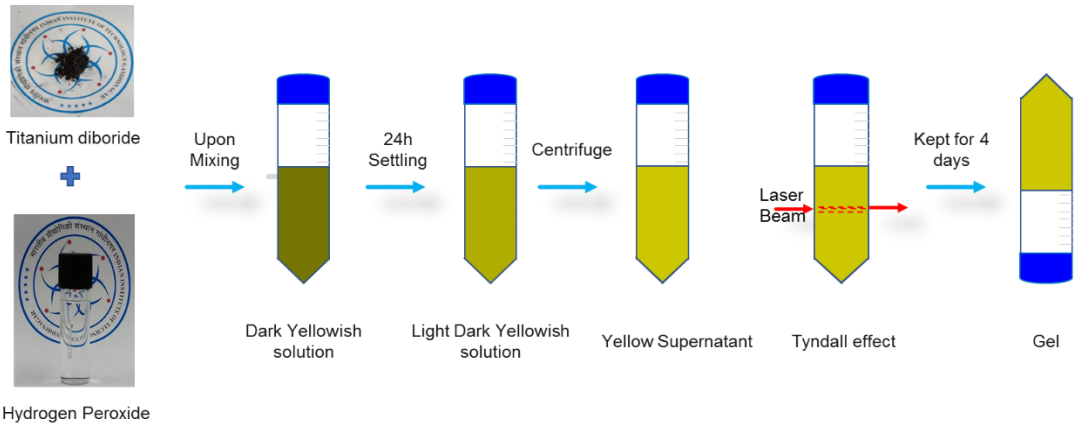

Figure 2. 1 Schematic representation of gel formation upon simple addition of titanium diboride to hydrogen peroxide

2.2 Observation:

When the same experiments were carried out again, then the gel didn't form after five days. Then the process was rechecked, and it was found out that two factors have been changed. First one was the change in the hydrogen peroxide brand, and the second one was the time of opening of the bottles. The new hydrogen peroxide bottle was purchased from Merck Life Science Limited, which was freshly opened while the previous hydrogen peroxide was from SD Fine Chem Limited, which was opened six months ago.

2.2.1 Possible mechanism of not forming a gel:

The hydrogen peroxide from S D Finechem Limited (SDFCL) was kept for a longer time, so when we add 10 ml of it, the gel formation was taking place. But when we were adding 10 ml of hydrogen peroxide (Merck Life Science Limited), which was purchased newly, it was not helping in the gelation. From the mechanism of decomposition of hydrogen peroxide, it is found that hydrogen peroxide disintegrates into water and oxygen with time.[42] So, the hydrogen peroxide from Merck, which was purchased new will have a higher number of H_2O_2 molecules as compared to the SDFCL one. Thus, we realized that we need to decrease the concentration of hydrogen peroxide when it is fresh, indeed to get the gelation.

2.3 Improvised recipe of gelation:

As the gel was not forming when we repeated the same experiments, we decreased the concentration of hydrogen peroxide to get the gel. The hydrogen peroxide concentration was intentionally decreased as x, x/2, x/3, x/4, x/5, and x/6 ml (where x=3.33 ml in 35 ml of H_2O and 100mg of TiB_2). Table 2.1 indicates, the variation in the concentration of reactants, which were tried to obtain gelation.

Sample No.	Ultrapure type I water (ml)	Titanium diboride(mg)	Hydrogen peroxide (Merck Life Sc. Ltd.) (ml)	Approximate ratio of TiB_2 to H_2O_2 (mg/ml)
1	35	100	3.33 = x	30
2	35	100	1.665 (x/2)	60
3	35	100	1.11 (x/3)	90
4	35	100	0.832 (x/4)	120
5	35	100	0.666 (x/5)	150

6	35	100	0.555 (x/6)	180

Table 2. 1 Variation in concentration of reactants for the formation of gel from the colloidal dispersion, the ratio of TiB_2/H_2O_2 was varied from 30 to 180 to get the gel as gel did not form after certain days.

2.3.1 Modification of parameter:

The previous recipe was 2 hours of stirring time followed by 24 hours settling, and centrifugation, which always resulted in a large quantity of unreacted titanium diboride. So, a modification in the stirring time was done, which resulted in a decrease of unreacted titanium diboride. Thus all the tabulated experiments which are given in Table 2.1 were carried out with an increased stirring time of 24 hours. Also, It is observed that the viscosity of the sample increased after the 24-hour reaction due to an increase in the concentration of the particles in the dispersed phase.

Sample Preparation:

Hydrogen Peroxide (SD Fine Chem Limited, 30% (w/w)) was added to the suspension of 100 mg of Titanium diboride (Sigma Aldrich, particle size < 10 µm and density= 4.52 g/ml) and 35 ml of water (Millipore Ultrapure Type I, Specific resistivity= 18.2 MΩ cm) in different concentrations. The solution was subjected to stirring for 24 hours with a speed of 250 rpm.

Centrifugation: The solution obtained after stirring was subjected to centrifugation (Thermo Fisher Scientific's Sorvall Legend X1R Centrifuge) at a speed of 8000 rpm for 15mins, at 20 ^{o}C. Then the supernatant was collected.

Two ml of the supernatant obtained after centrifugation in the above experiments (Table 2.1) were kept in 5 ml centrifuge tubes for further observation. The solution was observed each day, and after two days, it was found that when the tubes were inverted, the solution in the sample fell or partially fell or remain attached. The sample where TiB_2/H_2O_2 was 30, fell. The solution of the samples where TiB_2/H_2O_2 were 60, 180, and 150, partially fell. The solution of the samples where TiB_2/H_2O_2 was 90, and 120, remain attached to the tubes. But to the naked eye, it was

found out that the sample having TiB_2/H_2O_2 90 has a higher potency than the sample having TiB_2/H_2O_2 120. So the sample where TiB_2/H_2O_2 = 90 was selected as the final concentration for further analysis. Figure 2.2 showing the process involved in deciding the sample, which will give faster gelation.

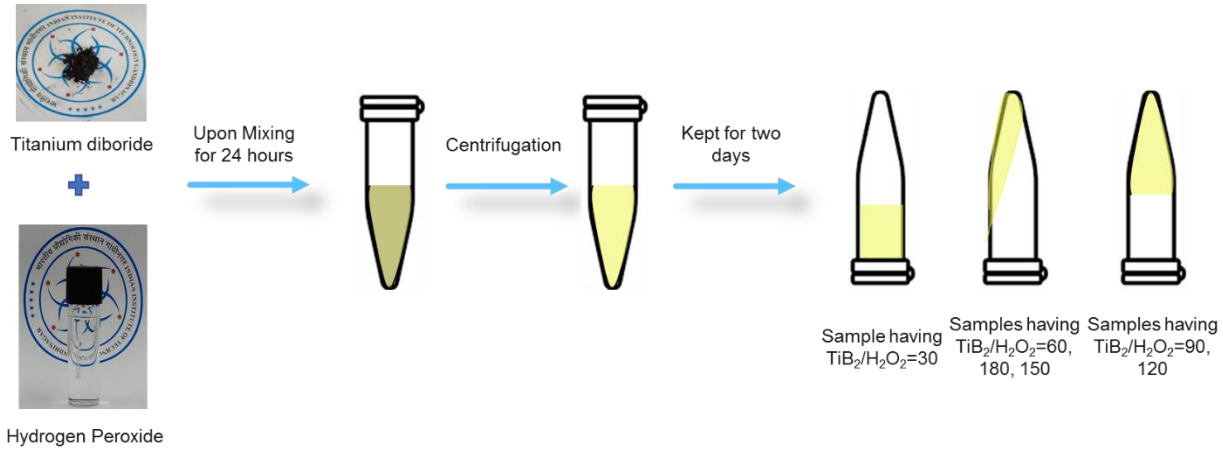

Figure 2. 2 Schematic diagram for finding gel formation recipe showing the samples having TiB_2/H_2O_2 of 30 remains as a liquid as the solution dropped after inverting. Whereas the sample with TiB_2/H_2O_2 of 60, 180, and 150 partially drop when inverted. The samples having TiB_2/H_2O_2 of 90 and 120 forms a gel as they remain attached to the tube after inverting.

2.3.2 Process modification:

The hydrogen peroxide is very corrosive, so we thought of removing it from the samples. The dialysis step was carried out to remove the unreacted hydrogen peroxide molecules.

Sample Preparation

1.11 ml of Hydrogen Peroxide (SD Fine Chem Limited, 30% (w/w)) was added to the suspension of 100 mg of Titanium diboride (Sigma Aldrich, particle size < 10 µm and density= 4.52 g/ml) and 35 ml of water (Millipore Ultrapure Type I, Specific resistivity= 18.2 MΩ. × cm). The solution was subjected to magnetic stirring for 24 hours with a speed of 250 rpm.

Centrifugation: The dark yellowish color obtained after stirring was subjected to centrifugation (Thermo Fisher Scientific's Sorvall Legend X1R Centrifuge) at a speed of 8000 rpm for 15mins, at 20 ^{o}C. The supernatant was collected, which is yellow.

Dialysis: Snakeskin dialysis tube having molecular weight cut-off (MWCO) of 10,000 kDa was used. The dialysis was conducted for 24 hours against deionized water, and the water was changed at an interval of 4 hours to increase the concentration gradient so that mass transfer of hydrogen peroxide molecules will be fast.

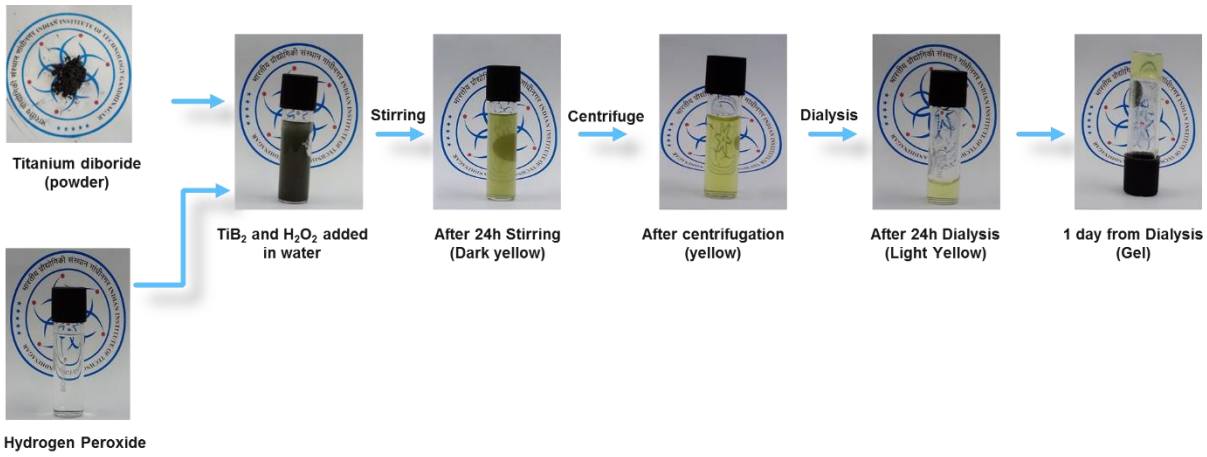

Figure 2. 3 Schematic of the Gel formation in the improvised recipe

The above recipe gives gelation within three days, starting from the synthesis. If we discard the dialysis process, then also we get the gel within three days. But later, it was even found out that the gel formation is occurring even after the dialysis process, which is shown in the rheology studies in chapter 4.

Once the recipe was established, then the different samples were analyzed at various intervals, as shown in table 2.2. These samples at the various intervals were analyzed directly or in powder form to get more insights on gel formation.

Sl. No.	Samples were taken
1	After 5 minutes of reaction
2	After 24 hours of reaction
3	After 12 hours of dialysis
4	After 24 hours of dialysis
5	After one day post dialysis
6	After two days post dialysis
7	After four days post dialysis
8	After six days post dialysis
9	After eight days post dialysis

Table 2. 2 Samples taken at different intervals

Lyophilization:

The sample (15ml in a falcon tube) was subjected to the freezing (–60 °C in Esco Lexicon ULT Freezer) for 24 hours, and this is followed by the lyophilization (CHRIST, Alpha 2–4 LD plus lyophilizer) at -85.5 ^{o}C, 0.5 mbar, 72 hours. The powder having yellowish white color was obtained after lyophilization. The lyophilized powders and the gels were characterized for further studies.

2.4 Characterization:

2.4.1 Structural characterization:

FESEM Analysis:

The model JEOL (JSM-7600F) Field-emission scanning electron microscope was used for FESEM analysis. The accelerating voltage is changed from 3 to 6 kV to capture the good quality images. The powder form of nanostructure was sprinkled on the conducting carbon adhesive tape, which was placed on the metal stub. Then the sample was sputter coated with platinum in a high vacuum chamber for about 70 s to form an ultra-thin layer, which was used for making the sample conductive.

XRD Analysis:

The X-ray diffraction (XRD) analysis was performed on a Bruker D8 Discover diffractometer using Cu Kα radiation of wavelength 1.54 Å. The scans were carried out with a step size of 0.02°, with 2θ ranging from 5° to 90°, and a scan speed of 0.2 s/step with a 40 V, 30 mA power.

2.4.2 Chemical characterization:

FTIR Spectroscopy:

The FTIR spectra were recorded on a Perkin Elmer Spectrum Two Spectrometer equipped with ATR accessory. A small amount of lyophilized powder was placed on the diamond crystal of the ATR accessory, and a proper force is applied through force gauge for getting the spectrum noise free. All the readings have been taken in the wavenumber range from 400 cm^{-1} to 4000 cm^{-1}

2.5 Results and discussion:

The reaction between titanium diboride and hydrogen peroxide resulted in a dark yellow colored solution. The centrifugation of this solution resulted in the yellow color supernatant and the black color sediments. The black color sediments are attributed to the unreacted titanium diboride particles. The supernatant is then subjected to the dialysis process, which removes the unreacted hydrogen peroxide molecules. The solution after dialysis results in light yellow color. When this was kept for one day, it forms a gel which can be seen in figure 2.4(a).

This gel exhibits the strong Tyndall beam effect, which indicates the presence of the dispersed phase. The dispersed phase is obtained in powder form through the lyophilization, which has a yellowish white color. The existence of nanosheets in the dispersed phase of the gel, which can be seen in the FESEM image of the lyophilized powder (figure 2.4(c)). The morphology of the nanosheets indicates that the exfoliation of the layered titanium diboride might have happened. But it is found out that the lateral dimension of the sheets is found to be around 100 µm, which is significantly larger than the size of the starting titanium diboride crystals (the maximum particle size is 10 µm). This suggests that something else might be happening in our system, as through exfoliation, we can not get sheets having a lateral dimension greater than the size of the titanium diboride, which is discussed in chapter 3.

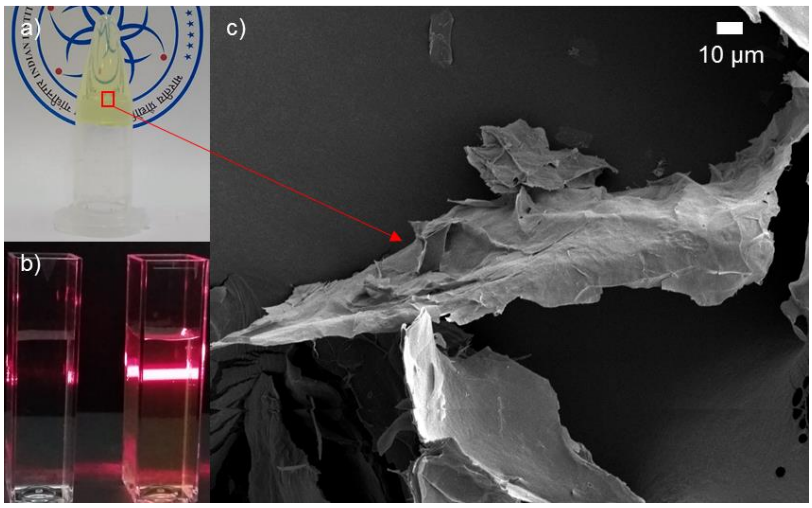

Figure 2. 4 Characterization of dispersed phase (a) Gel, (b) Gel showing Tyndall beam effect, (c) FESEM images of the lyophilized form of the gel indicating the presence of nanosheets

2.5.1 Analysis of different samples through characterization:

The various samples were prepared by varying the ratio of TiB_2 to H_2O_2, as given in table 2.1. These samples were then analyzed at different times, as given in table 2.2.

2.5.1.1 Analysis of samples after 4 hours of reaction:

After 4 hours of stirring, the solutions were taken for centrifugation, which is followed by lyophilization to get the dispersed phases in the form of powders. Then these powders were used for characterization like FESEM, FTIR, and XRD to see the difference between them.

FESEM Analysis:

The morphology of different samples after 4 hours of reaction can be seen in figure 2.5. It is found out that sheets are even forming after 4 hours of reaction in all cases except when the sample is prepared by using TiB_2/ H_2O_2 of 30. In this sample, flakes kind of structure, are obtained. Also, we are getting some nanowools or fibrous structure on the nanosheets in all samples.

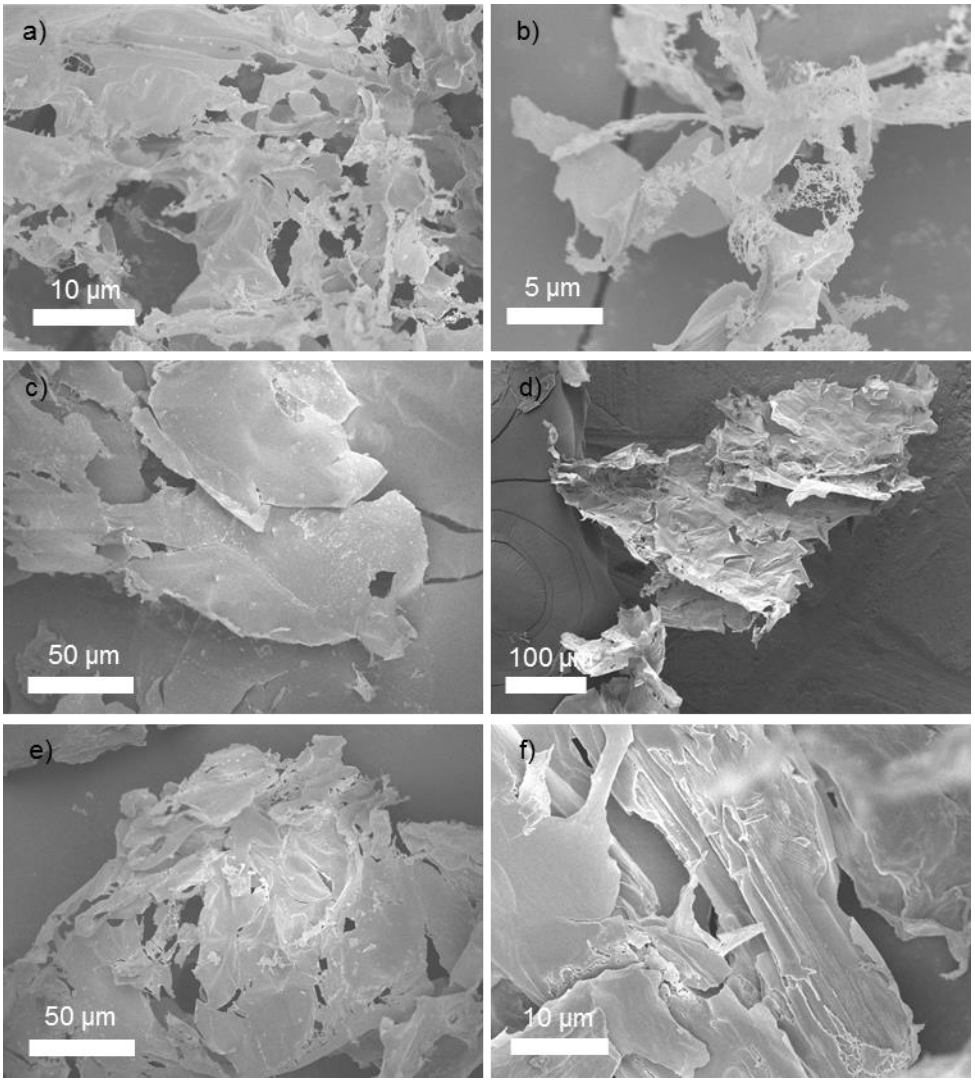

Figure 2. 5 FESEM images showing variation in the morphology of the samples prepared by reacting for 4 hours with varying the ratio of TiB_2 and H_2O_2. (a, b, c, d, e & f) FESEM images of the lyophilized powders of the samples where TiB_2/H_2O_2 is 180, 150, 120, 90, 60, & 30, respectively. (a, b, c, d, & e) showing the presence of nanosheets and a few amounts of nanowools; (f) showing the presence of nanoflakes.

FTIR Analysis:

The FTIR spectra indicate the presence of stretching of H-OH or B-OH bonds at the peak of 3202 cm^{-1}. This peak has broadened, which suggest the presence of hydrogen bonding. The peaks at 1625 cm^{-1}, 1408 cm^{-1}, 1190 cm^{-1}, 904 cm^{-1}, 694 cm^{-1}, and 634 cm^{-1} correspond to the presence of bending of OH groups in water or Ti-OH, stretching of B-O in BO_3, stretching of B-O in BO_4,

stretching of borate groups and stretching of Ti-O respectively. It is found out that the stretching of Ti-OH is absent in the samples of TiB_2/H_2O_2 =30 after four hours of reaction.

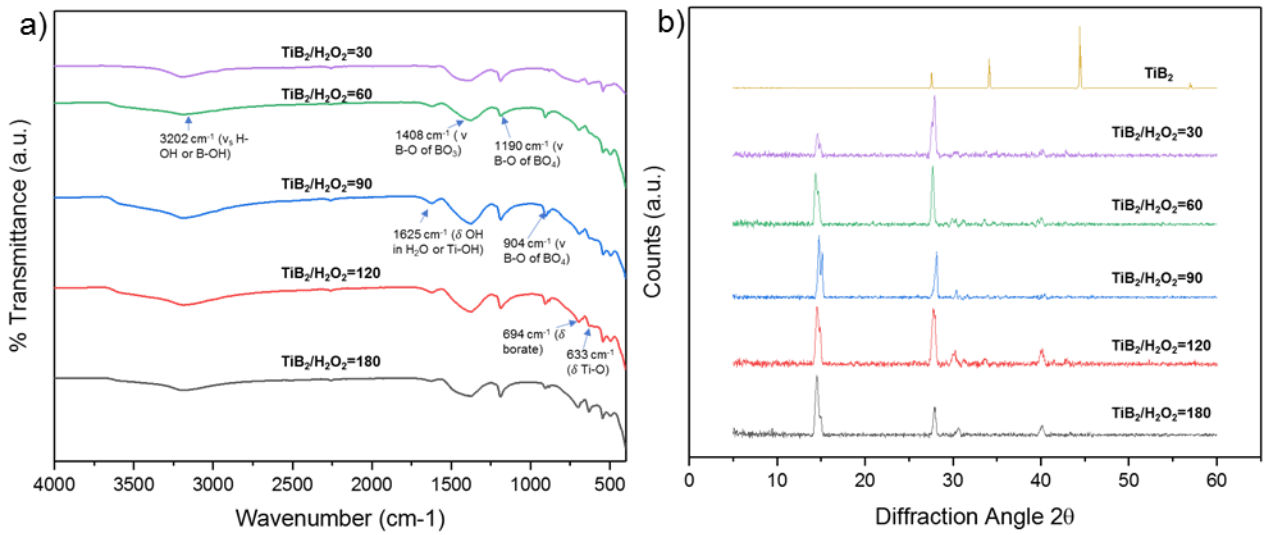

Figure 2. 6 (a)FTIR Spectrum of various samples after 4 hours of reaction; (b) XRD Spectrum of various samples after 4 hours of reaction

XRD Analysis:

The peaks are found at angles of 14.7^0, 15.1^0, 28.1^0 which corresponds to a d-spacing of 5.848 Å, 5.999 Å, and 3.165 Å respectively. These peaks are found in all the chemically modified samples. The peaks at 28.1^0 correspond to the presence of TiO_2, which can be found in the above samples.[43] The presence of TiO_2 matches with results from the FTIR. But as we are decreasing the concentration of hydrogen peroxide, the other peaks at 30.1^0 and 40.4^0 are becoming dominant as we can see from the samples where the TiB_2/H_2O_2 is 120 and 180. The peaks at 2θ of 30.1^0 and 40.4^0 correspond to a plane having d-spacing of 2.96 Å and 2.23 Å respectively. It is expected to study further to analyze the peaks at different positions near the future.

2.5.1.2 Analysis of samples after 24h of reaction:

After 24 hours of stirring, the solutions were taken for centrifugation, which is followed by lyophilization to get the dispersed phases in the form of powders. Then these powders used for characterization like FESEM, FTIR, and XRD to see the difference between them.

FESEM Analysis:

The morphology of different samples after 24 hours of reaction can be seen in figure 2.7. Figure 2.7(a, b, c, & d) showing the presence of more nanowools, which belongs to the sample when TiB_2/H_2O_2=180, 150, 120, & 90, respectively. Thus we can say that increasing the ratio of TiB_2/H_2O_2 results in more nanowools. Also, it is found out that the samples where TiB_2/H_2O_2=30 is forming nanosheets after 24 hours of reaction, but there were no sheets after 4 hours of reaction. So, we can say that the decrease in the TiB_2/H_2O_2 results in a slow synthesis of nanosheets.

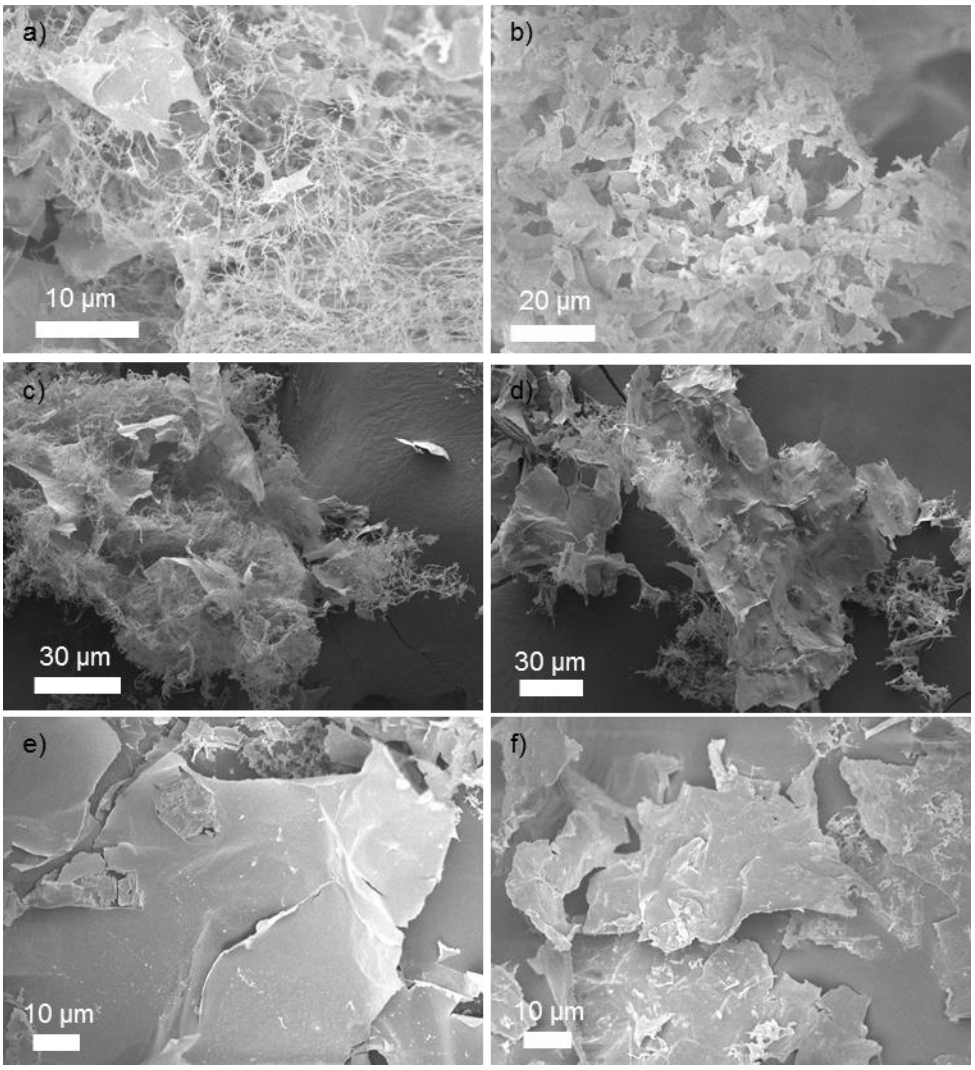

Figure 2. 7 FESEM images showing variation in the morphology of the samples prepared by reacting for 24 hours with varying the ratio of TiB_2 and H_2O_2. (a, b, c, d, e & f) FESEM images of the lyophilized powders of the samples where TiB_2/H_2O_2 is 180, 150, 120, 90, 60, & 30, respectively. (a, b, c, & d) Showing the presence of some nanosheets and bunch of nanowools; (e, & f) showing the presence of nanosheets with very less or no nanowools. This suggests that decreasing the ratio of TiB_2/H_2O_2 results in fewer nanowools.

FTIR Analysis:

The FTIR spectra indicate the presence of stretching of H-OH or B-OH bonds at the peak of 3202 cm^{-1}. This peak has broadened which suggest the presence of hydrogen bonding. The peak at 1625 cm^{-1}, 1408 cm^{-1}, 1190 cm^{-1}, 904 cm^{-1}, 694 cm^{-1}, and 634 cm^{-1} corresponds to the presence of bending of OH in water or Ti-OH, stretching of B-O in BO_3, stretching of B-O in BO_4, stretching

of borate groups and stretching of Ti-O respectively. Here there is the presence of Ti-OH bonds after 24 hours of reaction in the samples where TiB_2/H_2O_2 =30. It suggests that the Ti-OH bonds form with time.

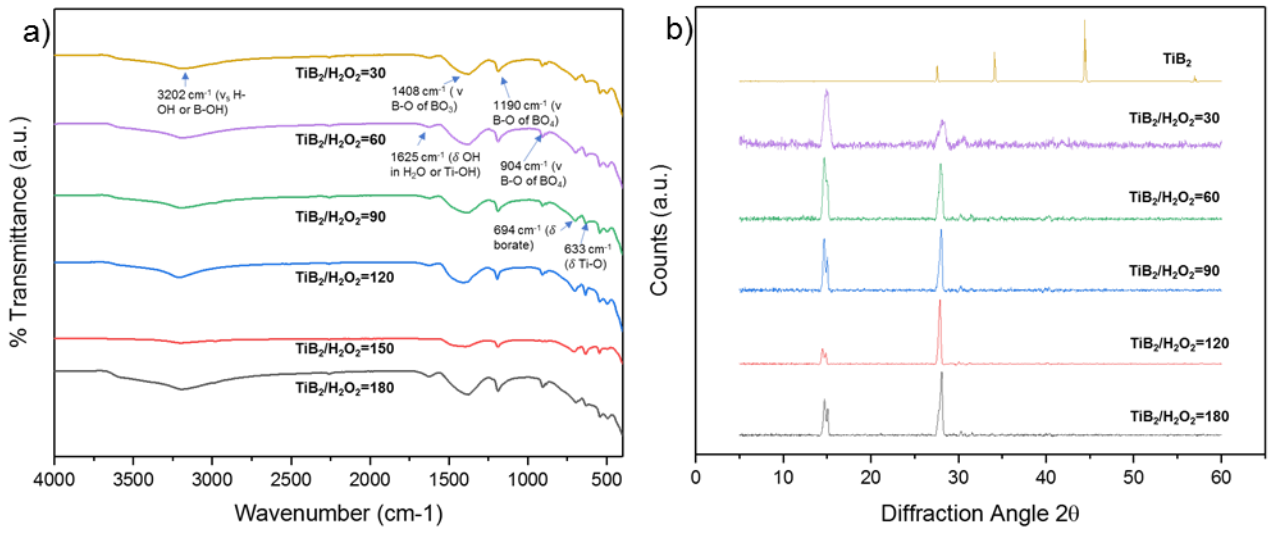

Figure 2. 8 (a)FTIR Spectrum of various samples after 24 hours of reaction; (b) XRD Spectrum of various samples after 24 hours of reaction

XRD Analysis:

Similar peaks are found at an angle of 14.7^0, 15.1^0, and 28.1^0 (TiO_2), which corresponds to a d-spacing of 5.848 Å, 5.999 Å, 3.165 Å respectively in the samples after 24 hours of reaction. These peaks are found in all the chemically modified samples. The peaks that were found in the samples (TiB2/ H2O2= 120, 180) after 4 hours of reaction at a 2θ of 30.1^0 and 40.4^0 is vanishing after 24 hours of reaction. This suggests that some intermediate compound is forming after 4 hours of reaction, which is vanishing after 24 hours of reaction. The detailed analysis can be done further in the future.

2.5.2 Characterization of selected samples:

The samples having TiB_2/H_2O_2=90 is chosen as the finalized recipe because of faster gelation (The gel forms after just one day of post-dialysis). It is found out that the yield of nanostructures is very high, that is 3 mg per ml. This is because of all the titanium diborides are reacting, and a very a little amount of titanium diboride is found after the reaction process.

This sample is characterized through FESEM, FTIR, and XRD to get more insight into the gel formation.

FESEM Analysis:

The morphology of the samples was studied through FESEM by taking samples at different intervals during the synthesis process and post-synthesis process like after 5 minutes of reaction, after 4 hours of reaction, after 24 hours of reaction, after 12 hours of dialysis, after 24 hours of dialysis, and after one day of post dialysis. Figure 2.10 shows the morphology of the above samples. It is found out that nanosheets are even forming after 5 minutes of reaction (figure 2.10a).

Along with the nanosheets, some nanowools are forming (mostly starts after 24h of reaction- figure 2.10c). A large number of nanowools can be seen mostly after 12 hours of dialysis in the samples, figure 2.10d. These nanowools then aggregated with time (mostly start to happen after 24h of dialysis) and deposited on the nanosheets, which result in the wrinkle on the sheets (mostly seen after post dialysis). All the process of forming nanowools, aggregating with each other, and depositing on the nanosheets is found to be present simultaneously at every interval of samples, which is described in chapter 4.

FTIR Analysis:

The Fourier transform infrared analysis of the samples have been analyzed to get the insights of the functional groups of the samples with the processing time, which is shown in figure 2.9(a). It was found out that the peak at 1625 cm^{-1} corresponds to the bending of Ti-OH is becoming prominent with time during and after the dialysis process. Also, it is observed that the peaks at 1408 cm^{-1} and 1190 cm^{-1}, which corresponds to the stretching of B-O in BO_3 and BO_4 respectively vanish with time during and after the dialysis process.

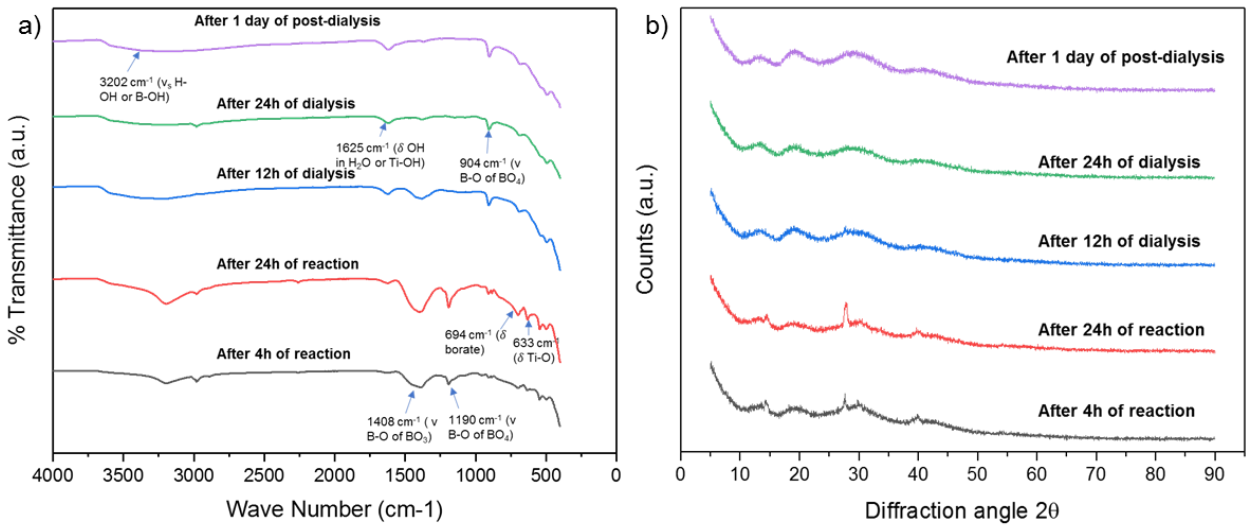

Figure 2. 9 (a) FTIR Spectrum of the faster gel formation sample at different times; (b) XRD Spectrum of various of the same samples at different times

XRD Analysis:

The peaks are found at an angle of 14.70^0, 15.10^0, and 28.10^0, which corresponds to a d-spacing of 5.848 Å, 5.999 Å, and 3.165 Å respectively after the reaction, which tells us that the sample is purely crystalline after the reaction. But when we are doing dialysis, the intensity of the peaks is vanishing, which can be seen from figure 2.9(b) and the compound is converted more towards amorphous. Also, the peak at 28.10^0 corresponds to the TiO_2 compound[43], and the other peaks can be analyzed in the future.

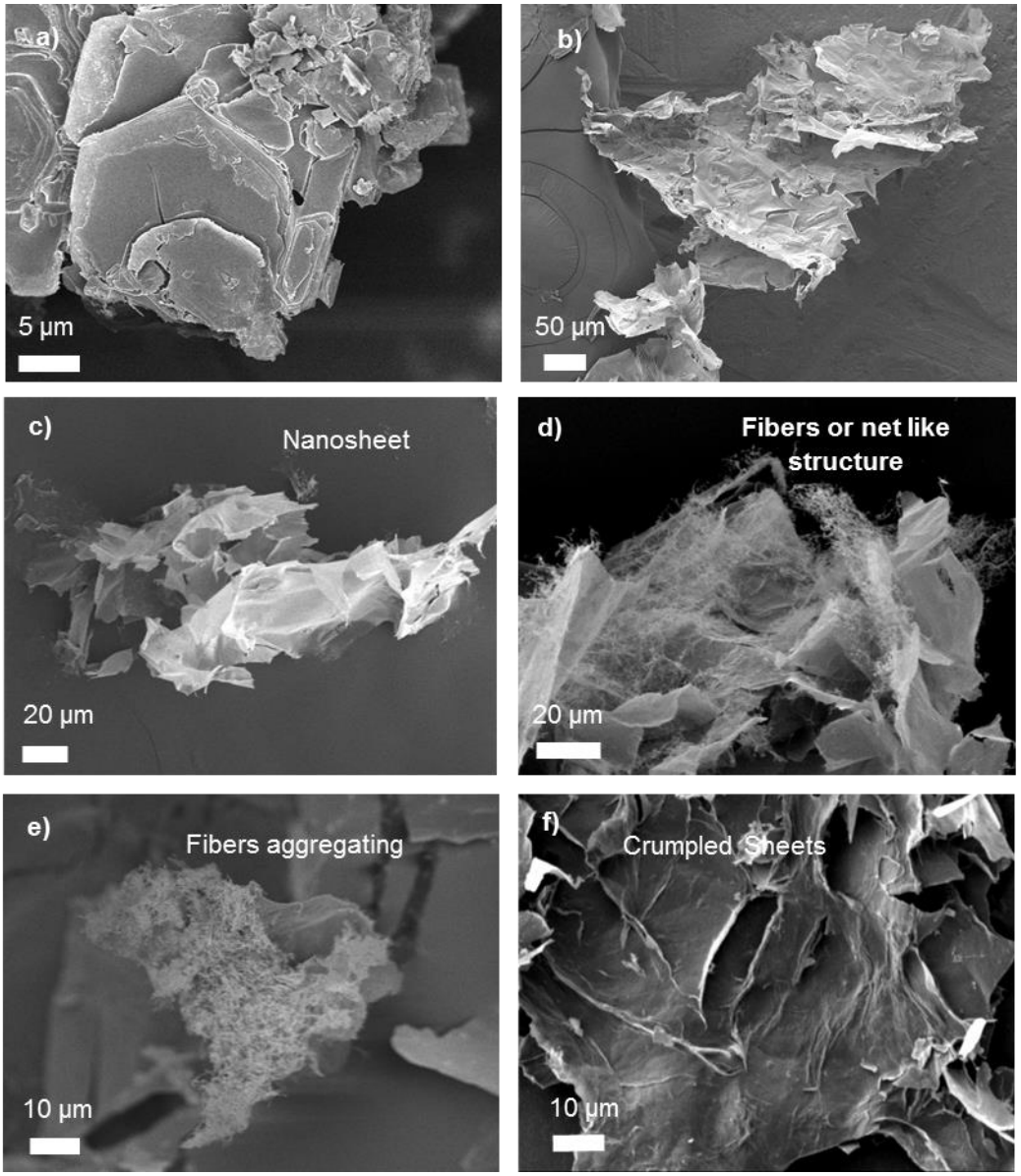

Figure 2. 10 FESEM images showing variation in the morphology with the processing time of gel after lyophilization. (a, b, c, d, e, & f) Powders obtained after 5 mins of reaction, 4h of reaction, 24h of reaction, 12h of dialysis, 24h of dialysis, & one day of post-dialysis respectively. All the images describing the formation of nanowools, their aggregation, and their deposition on the nanosheets, which results in the wrinkle formation

2.6 Conclusion:

The reaction between titanium diboride and hydrogen peroxide resulted in a different gradient of yellow color solution. This solution only forms a gel in a particular concentration range. It is

found out that when we are mixing 1.11 ml of hydrogen peroxide to the solution of 100 mg titanium diboride and 35 ml of water for 24 hours, then the gelation occurs at a fast rate. Also, it is found from the FESEM that the dispersed phase consists of both nanosheets (the lateral dimension, which is very greater than the size of the titanium diboride) and nanowools. The yield of the nanostructures is high, that is 3 mg per ml. The concentration of both the nanosheets and nanowools depend upon the amount of reactant added, and the processing time. It is noticed from the FESEM images that the nanowools are aggregating with each other and deposited on the surface of the nanosheets, which result in the formation of wrinkles on the surface of the sheets. As the samples having TiB_2/H_2O_2= 90 (TiB_2=100mg, H_2O_2=1.11 ml) gives the faster gelation, so it is analyzed further to know about the mechanism of the gelation and the reason behind the formation of large sheets.

Chapter 3: Insights into the Gel formation

3.1 Introduction:

We optimize the parameter and the synthesis process to get the hydrogel in one day. During the synthesis, we found that the colloidal dispersion consists of large sheets, whose lateral dimensions were higher than the initial size of TiB_2 crystals. Here we discuss the possible mechanism for the formation of large dimension sheets, which is found after the time-dependent studies. Here the samples were studied under TEM/HRTEM at different time intervals. The TEM analysis revealed a unique possibility for the sheet formation that is a bottom-up approach. In addition, we propose the possible mechanism of the gel formation, which is found through zeta potential studies and reduction studies. Reduction study is followed by the reduction of the hydrogel and the FTIR analysis of the reduced sample, which gives us the details about the crosslinking networks in the hydrogel. Then we discuss the Raman analysis to see whether the nanosheets have boron honeycomb planes. Also, we examine the presence of large sheets through an optical microscope and an atomic force microscope. In addition, the thermal properties of the nanostructures are analyzed through TG-DSC.

3.2 Time-dependent studies:

The gel formation is a time-dependent process, so the sample was analyzed at different time intervals to study the gel formation.

3.2.1 Characterization:

TEM Analysis:

The lacey carbon coated on a 300 mesh copper grid from Ted Pella was used. The samples for TEM were prepared by placing a few drops of the dispersion on the parafilm tape and waving the TEM grid in the drop of the dispersion. Then to remove the excess dispersion from the TEM grids, it was touched vertically slightly to the tissue papers, and through capillary action, the excess dispersion sample was removed. Then the grids were placed on the grid box for drying at room temperature. TEM/HRTEM images were obtained by using a JEM-2100F model.

The TEM/HRTEM analysis of the samples was done to get more insights into the formation of nanosheets. The samples have been analyzed after 5 minutes of reaction, 24 hours of reaction, 12 hours of dialysis, and 24 hours of dialysis under TEM. We are able to get the images in the sample after 5 minutes and 24 hours of reaction. But, the samples after 12 hours of dialysis and 24 hours of dialysis are found to be heavily concentrated on the grids, so we could not get clear TEM images. Figure 3.1 shows the TEM and HRTEM images of the sample after 5 minutes of reaction. The HRTEM images in figure 3.1 (d, & e) reveal the presence of pre-nucleation clusters. It is found out that the aggregation of the small clusters is taking place, which results in the formation of large nanosheets and nanowools after 24 hours of reaction(figure 3.2)

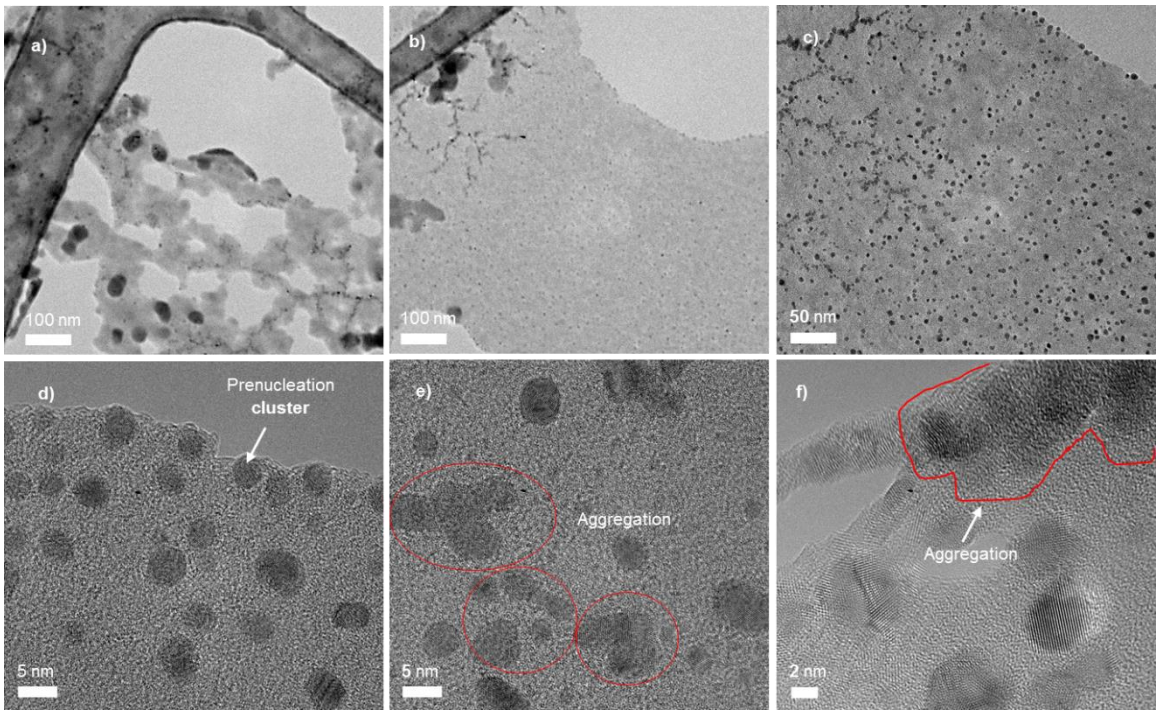

Figure 3. 1 TEM/HRTEM images showing the aggregation of small particles which results in the formation of large sheets. The sample is a yellow color solution after 5 minutes of the reaction. (a, b) Showing the clear growth through aggregation; (c, d) showing the presence of very small particles all over the solution; (e, f) growth or recrystallization is occurring, which result in the formation of nanosheets

.

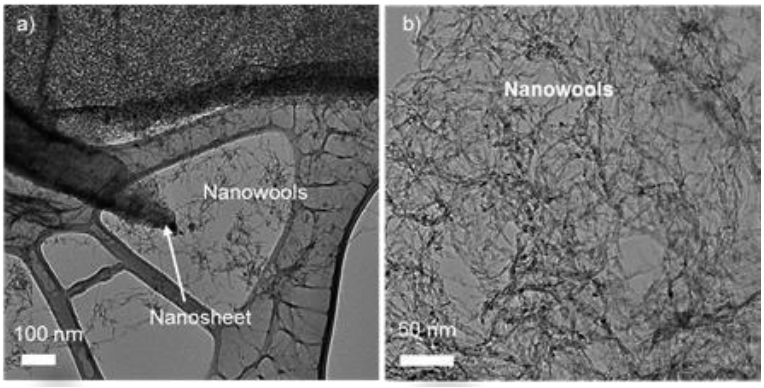

Figure 3. 2 TEM images of the sample after 24 hours of reaction showing the presence of both nanosheets and nanowools.

It is observed from the TEM and HRTEM analysis that the prenucleation clusters are present after five minutes of reaction. Then we are observing the presence of nanosheets and nanowools after 24h of reaction.

Similar observations of the formation of pre-nucleation clusters have made by Caetano et al., where they have shown that tin tetrachloride pentahydrate (SnCl4·5H2O) in absolute ethanol forms pre-nucleation clusters and these aggregates to SnO_2 nanoparticles.[44] Also, Gunda et al. have shown the formation of pre-nucleation clusters of MgB2 in water, which upon aging undergo non-classical crystallization preferentially growing in the lateral dimension.[30] The aggregation of these clusters generally occurs by oriented attachment (OA), which is widely accepted as non-classical growth.[45,46] From the thermodynamics point of view, oriented attachment is favored due to the decrease in the value of surface energy as the clusters are merging into a large structure.[47] OA enables to synthesize a single structure with well-defined size having dimensions of tens of micrometers with no or a few defects, which is only possible due to the fast diffusion of small clusters. [48]

Nanoparticles involved in Oriented attachment (OA) depends on the ligands, surfactants, or polymers. Schliehe et al. have shown that PbS nanoparticles synthesized in the presence of chloroalkanes, assemble in a 2D manner into a single crystal nanosheet.[49] Thus we can say that if there is a change in the ligands, surfactants, or polymers, then the OA can change.

In our case, the nanosheets and nanowools are forming by process of non-classical crystallization. The prenucleation clusters are formed due to the dissolution of titanium diboride in the presence of hydrogen peroxide molecules in water. Here the prenucleation clusters are subjected to the oriented attachment to have low surface energy, and the OA occurs in two ways (2D and 1D). The OA, which occurs in 2D results in the formation of nanosheets (here growth occurs in lateral dimension) and the OA, which occur through 1D results in the formation nanowools (here the growth occurs in one direction).

AFM Analysis:

Atomic force microscopy (AFM) images were obtained using the Bruker multimode 8. The images were acquired with the aid of a silicon cantilever (NSG 10-Tip, spring constant 3.08 Nm^{-1}, resonating frequency 140 kHz). The gel sample after one day post-dialysis was taken for analysis. The samples for AFM was prepared by immobilizing the sheets on the silicon wafers. Silicon wafers of 1 cm × 1 cm was taken for analysis. These wafers were cleaned with water, acetone, ethanol, isopropanol, and again with acetone in a bath sonicator. Each time, these wafers were dried with nitrogen gas. The oxygen plasma treatment (Power = 100 watts, time= 2mins, and pressure= two mbar) was done to these wafers. The surface of the wafers treated with a solution of 1% 3-aminopropyltriethoxysilane (APTES) in ethanol for 20 min. Then the wafers kept in the hot oven at 120^{o}C for 4 min. The gel sample was dispensed on the wafers and left undisturbed for five min. After five minutes, the wafers were cleaned thoroughly with water. Then the wafers were kept in the desiccator for drying for 24 hours. All the AFM images were analyzed using nanoscope software of version 1.40.

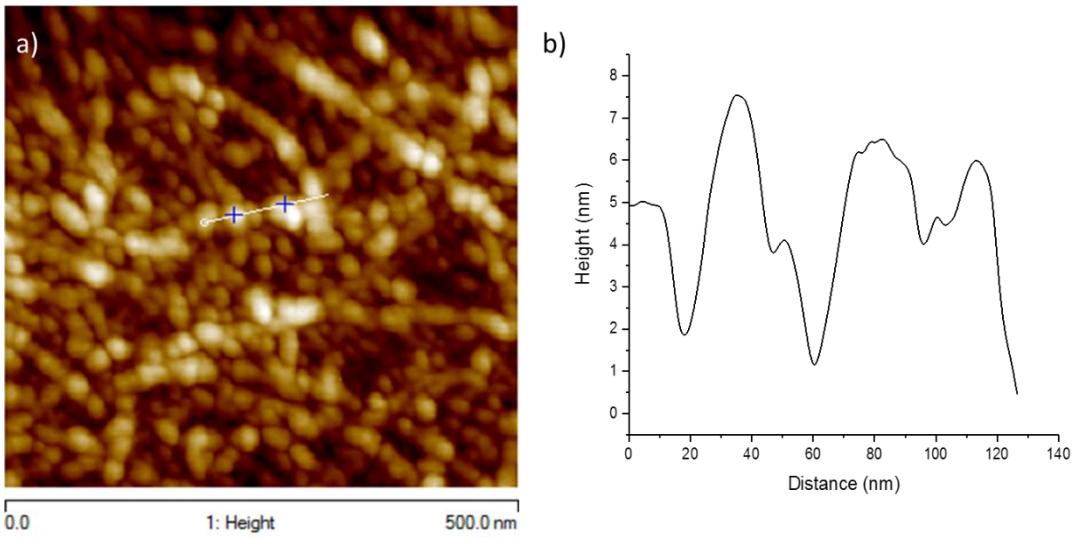

Figure 3. 3 AFM images of the gel samples prepared by immobilizing the sheets on the silicon surface. (a) showing the topography of the sheets; (b) indicating the roughness plot.

FESEM Analysis:

The model JEOL (JSM-7600F) Field-emission scanning electron microscope was used for FESEM analysis. The accelerating voltage is changed from 4 to 8 kV. The powdered form of nanostructure was sprinkled on the adhesive conducting carbon tape which was placed on the metal stub. Then the sample was sputter coated with platinum in a high vacuum chamber for about 70 s to form an ultra-thin layer, which was used for making the sample conductive.

From TEM analysis, we found that the nanosheets and nanowools were formed by growth but not by exfoliation. This leads us to investigate the 5 minutes of samples through FESEM. Figure 3.4 showing the morphology of powder sample after 5 minutes of reaction, which was lyophilized. We found that the growth of small particles is occurring, which results in the formation of nanosheets.

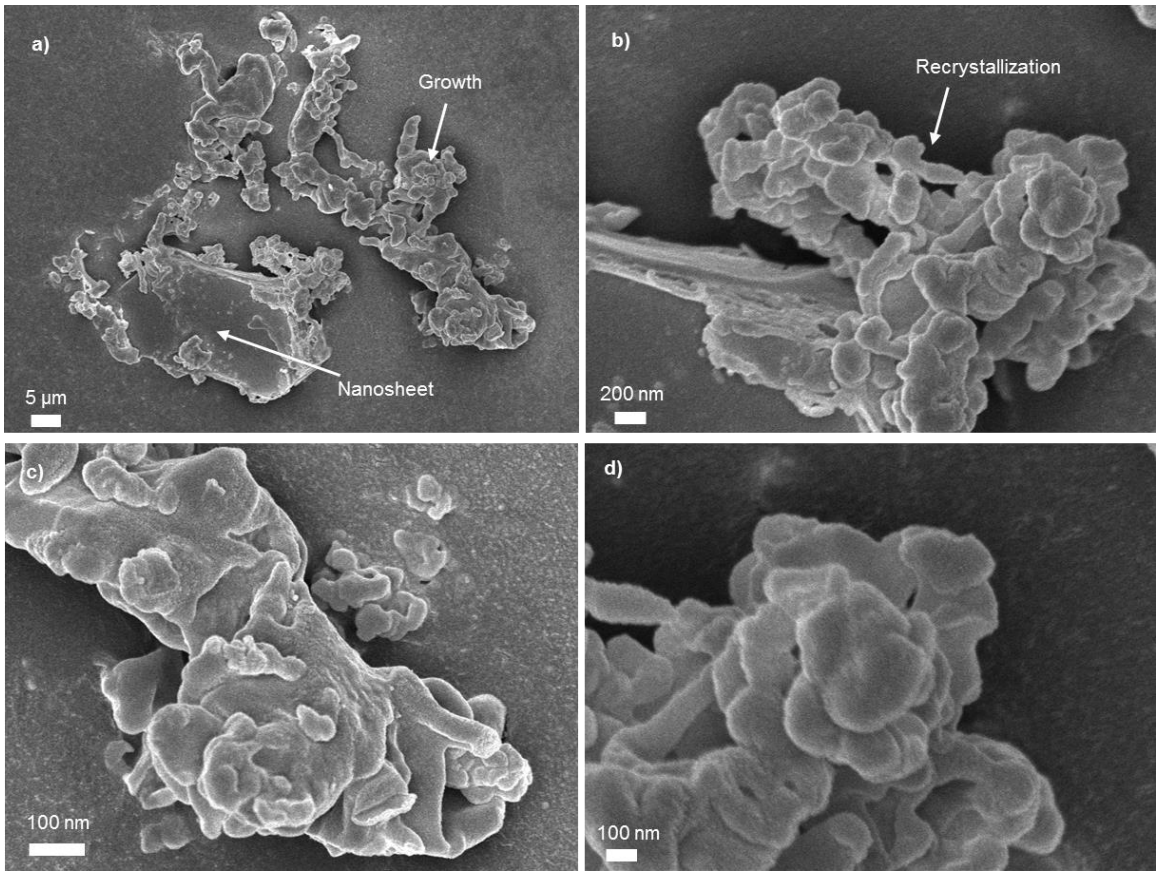

Figure 3. 4 FESEM images showing the morphology of the sample after 5 minutes of reaction. (a) Showing the clear presence of both nanosheets and growth; (b, c, & d) showing the growth or recrystallization is occurring, which result in the formation of large sheets.

3.2.2 Proposed mechanism for the formation of large sheets:

We found the presence of pre-nucleation clusters of diameters around 2 to 5 nm, as shown in figure 3.1 (d). These pre-nucleation clusters aggregate to form nanosheets and nanowools, as shown in figure 3.2 (a & b). So, we are proposing that the nanosheets are forming through a non-classical crystallization process[50], which is similar to the phenomenon reported by Gunda et al. in the case of MgB_2 crystals in water[30]. Here the titanium diboride powders first undergo dissolution in the presence of hydrogen peroxide and water and forms pre-nucleation clusters. These pre-nucleation clusters have very high surface energy, so they try to come to the lowers surface energy region by aggregating. We can say that dissolution is occurring, which is

followed by recrystallization. Here two types of growth are occurring as mentioned above. One is 2D oriented attachment growth, which results in nanosheets formation, and another one is 1D oriented attachment growth, which results in nanowools formation. The nanosheets growth in 2D oriented is found from the AFM analysis. Fig 3.3 (a & b) shows the topography of the gel and roughness profile in 120 nm range. The average roughness is coming around 4 nm, which is very small. This suggests that the growth in nanosheets is preferentially occurring in lateral dimension by 2D oriented attachment.[30,51,52]

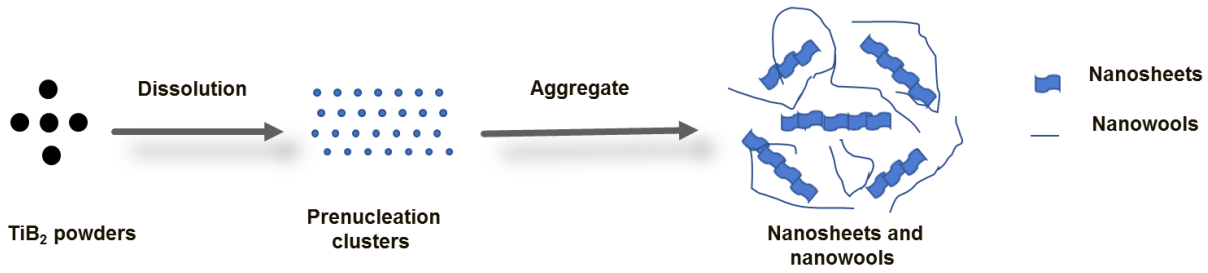

Figure 3. 5 Schematic showing the formation mechanism of large sheets, which indicates that the formation of large nanosheets and nanowools follow a non-classical crystallization path.

3.3 Mechanism of Gel formation:

The mechanism of gel formation is found by taking the assumption of different methods by which gel can form. It is found out that gel can form due to the electrostatic force of attraction, hydrogen bonding, and van der Waals force of attraction, etc.[53]

3.3.1 Electrostatic force of attraction:

Zeta potential studies were carried out in zeta potential analyzer (NICOMP, 380 ZLS) at different times to find out whether the gel is forming due to the electrostatic force of interaction or not.

Zeta Potential Analysis:

It is found out that the zeta potential is coming in between -47 to -57 mV, which is shown in figure 3.6. The zeta potential has been found out from the samples after 4h of reaction, after 24h of reaction, after 24h of dialysis, and after one day of post dialysis. It is found that there is no significant variation in zeta potentials. Also, It has been observed by Li et al. that beyond -30

mV is required to prevent particles aggregation.[54] The retention of a significant magnitude of zeta potential suggests that there is no loss of negatively charged particles during the process of gel formation, which indicates that the gel is not forming due to the electrostatic force of attraction. The similar phenomena have been observed in graphene oxide gel.[53]

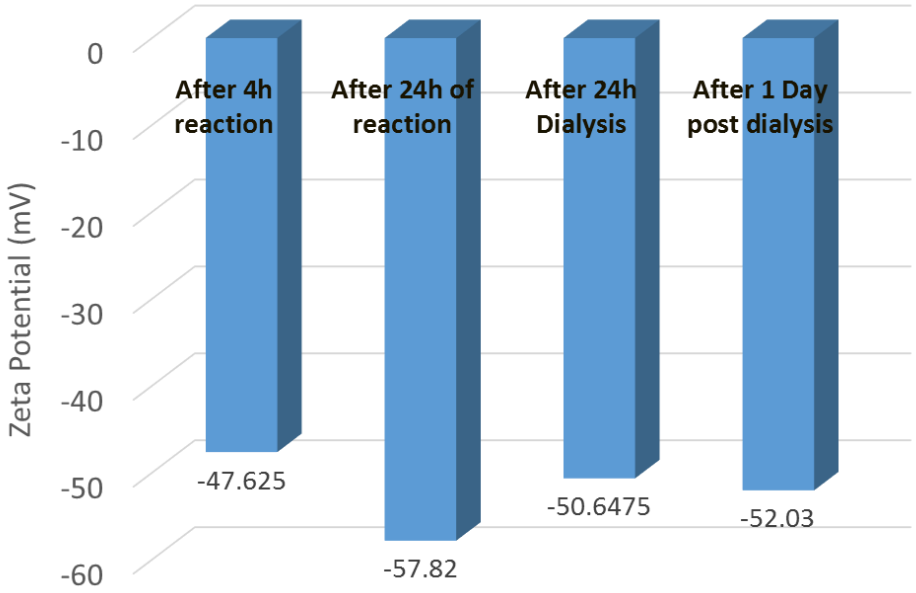

Figure 3. 6 Zeta Potential studies of the samples with time indicating no significant variation in the values

3.3.2 Chemical crosslinking:

As gel was not forming due to the electrostatic force of attraction, so it might be forming due to the chemical crosslinking between the functional groups or may be due to the van der Waals force of attraction.[53] We tried a reduction method to find out the answer to the question of the mechanism of gel formation.

Sodium borohydride ($NaBH_4$) was chosen as the reducing agent. When we added sodium borohydride to the gel, the gel is not remaining in its original shape. It is converted to the liquid. But as sodium borohydride contains boron, so it will create a problem in distinguishing the

boron in chemical characterization. Thus a reducing agent is chosen in which boron is not there, and it is not as harmful as sodium borohydride. Ascorbic acid is the most suitable for these criteria. So ascorbic acid is chosen as the reducing agent in this process.

3.3.2.1 Sample Preparation:

The stock solution of ascorbic acid was prepared by adding a specific amount to the deionized water (Millipore Ultrapure Type I, Specific resistivity= 18.2 MΩ.cm). The stock solution is prepared as 5 mg/ml, 10 mg/ml, 15 mg/ml, 20 mg/ml, 25 mg/ml, 30 mg/ml, 35 mg/ml, 40 mg/ml, 45 mg/ml, and 50 mg/ml. Then it is added to the gel and kept for 24 hours for observation.

Observation:

It is found out that the gel is converted to the liquid in each stock solution, and the color of the solution also changed to different gradients of orange colors. With the addition of a low stock solution of ascorbic acid, it is observed that the color of the solution is becoming light yellow, but in the addition of higher concentration of ascorbic acid, it becomes dark orange. As we are keeping the solution for 24 hours, it is becoming a reversible process by coming back to the original yellow color, and the sample is becoming viscous. This reversible process is observed in the sample where 5 mg/ml, 10 mg/ml, and 15 mg/ml of stock solution was added. No changes are seen through the naked eye in the sample, where a higher amount of stock solution was added. A stock solution of 45 mg/ml is chosen for the reduction process to be in a safety region.

Dialysis: SnakeSkin dialysis tube having molecular weight cut-off (MWCO) of 10,000 kDa was used. The dialysis continued for 24 hours against deionized water, and the water was changed at an interval of 4 hours to increase the concentration gradient so that mass transfer of hydrogen peroxide molecules will be fast.

Lyophilization: The sample (15ml in a falcon tube) subjected to the freezing (–60 °C in Esco Lexicon ULT Freezer) for 24 hours and this is followed by the lyophilization (CHRIST, Alpha 2–4 LD plus lyophilizer) at -85.5 ^{o}C, 0.5 mbar, 72 hours. The powder having orange-white color was obtained after lyophilization.

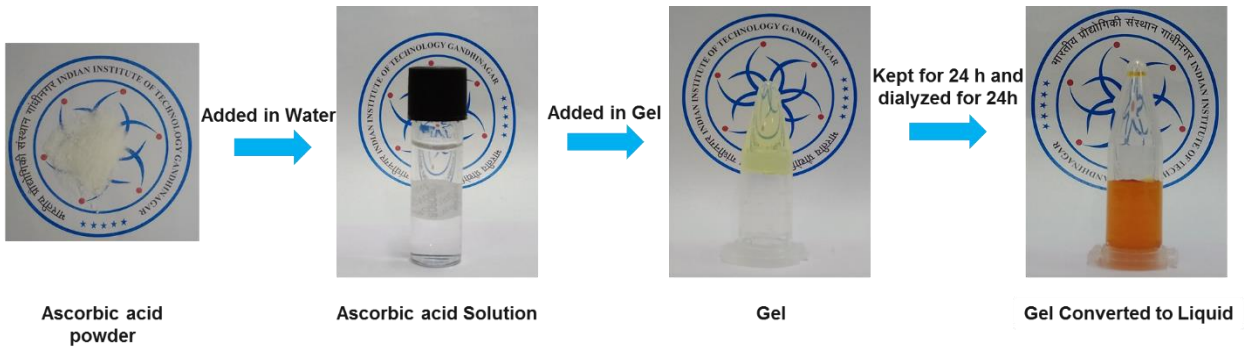

Figure 3. 7 Process of breaking the crosslinks by addition of ascorbic acid as a reducing agent

3.3.2.2 Results and discussion:

The reaction between the gel and the ascorbic acid solution resulted in an orange color solution, which also results in breaking the crosslinking in the gel. The sample was dialyzed to remove the excess ascorbic acid, which is followed by lyophilization. The orange-white color powder is obtained after lyophilization.

FTIR Analysis:

The gel has functional groups like of B-OH, Ti-OH, B-O in BO3 and BO4, and other borate groups at 3202 cm-1, 1615 cm-1, 1408 cm-1, 904 cm-1, and 694 cm-1 respectively. However, it is found that the only stretching of Ti-OH is remaining and other groups are vanishing after reduction, which indicates that the borate groups might be reduced in this process. We can say that with the reduction of functional groups, the gel is disappearing, which suggest that the gel is forming mainly due to the chemical crosslinking. As there is a loss of borate groups, so we can say the chemical crosslinking is mainly due to the borate groups.

FESEM Analysis:

It is found out the presence of large sheet in both reduced sample and dialyzed sample, which can be seen from figure 3.9 (a,b). This indicates that the nanosheets are remaining the same in both the gel and reduced sample. The prenucleation clusters are intact to each other in the nanosheets, which also suggest that the nanosheets are not made by chemical crosslinking, which is made up through oriented attachment as found above. Also, we can see the wrinkle

formation on the nanosheets, which is due to the deposition of nanowools, as discussed in chapter 2.

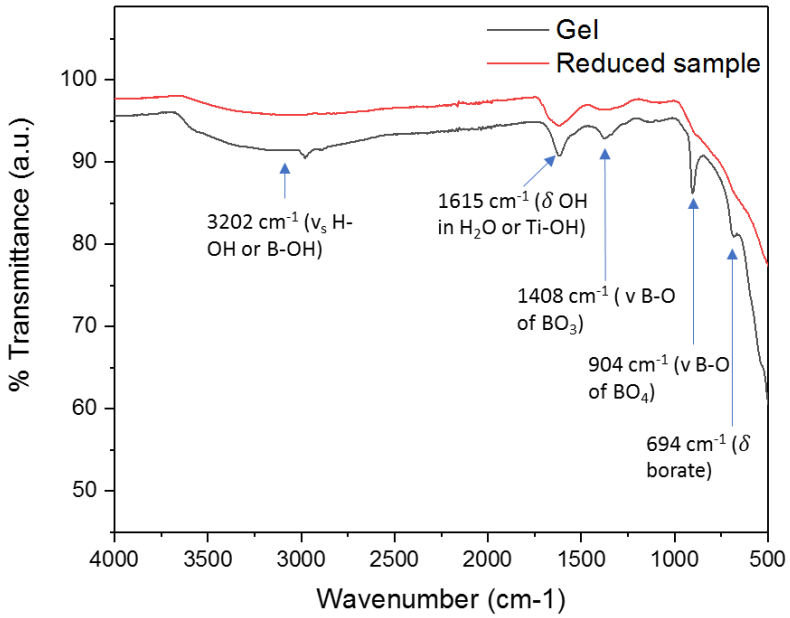

Figure 3. 8 FTIR of the gel and reduced sample

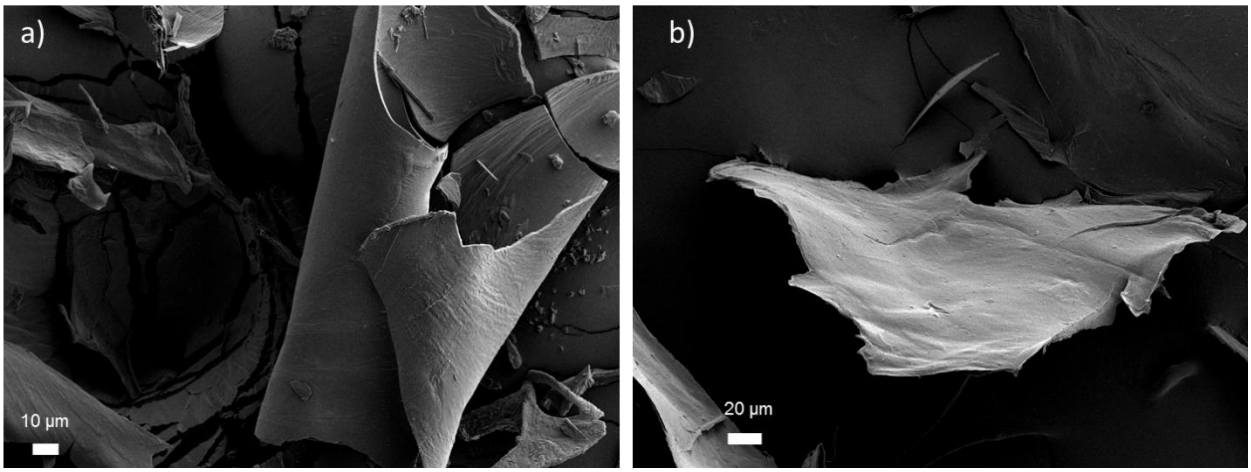

Figure 3. 9 FESEM of the reduced samples showing larger sheets in both a,b; (a) morphology of the reduced sample, (b) morphology of the reduced sample after dialysis. This indicates that the nanosheets observed in the gel are the same as in the reduced sample.

3.3.3 Proposed Mechanism of Gel formation:

According to the FTIR results from figure 3.8, it is found out that the nanosheets have been reduced. The reduced sample has only Ti-OH stretching, and no borate functional groups are there. So, It can be said that with the removal of borate functional groups, the gel is disappearing, which tells that the gel is forming due to the borate crosslinking. The above mechanism is described in figure 3.10. We know that our nanosheets contain various functional groups while remaining dispersed in the solution. Then these functional groups form crosslinking networks through the borate groups. Then the water gets trapped inside the networks resulting in the hydrogel formation.

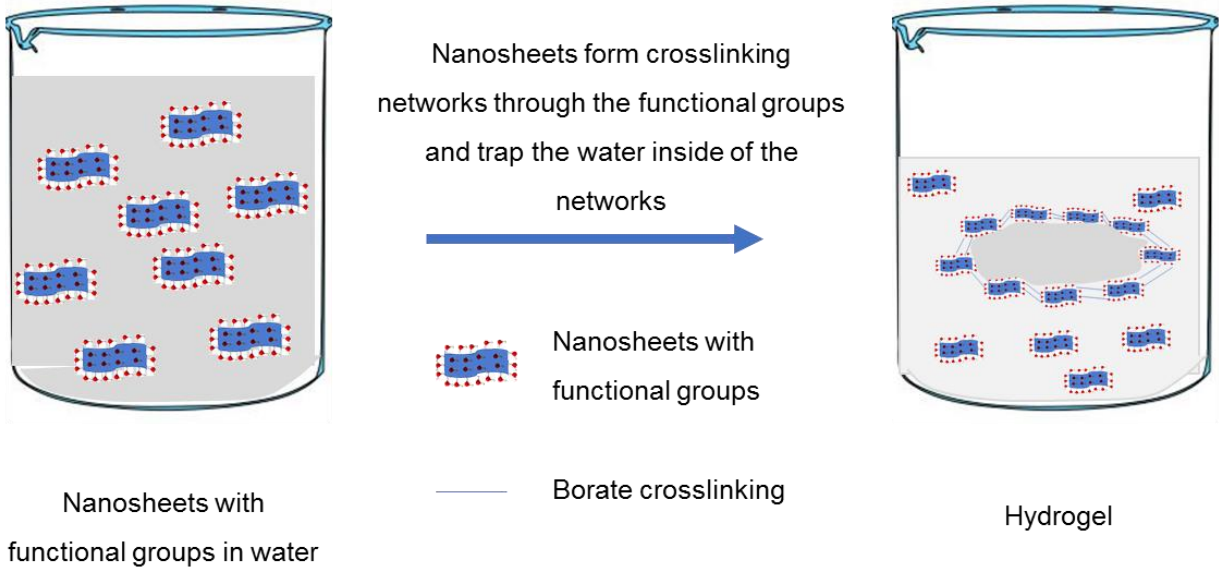

Figure 3. 10 Schematic diagrams showing the hydrogel formation through the borate crosslinking and the water is being trapped inside the networks.

3.4 Characterization:

3.4.1 Structural Characterization:

Optical Microscopy:

Olympus BX51TRF was used for the study. The samples were prepared by immobilizing the sheets on the silicon wafers. Silicon wafers were cleaned with water, acetone, ethanol,

isopropanol, and again with acetone. Each time, these wafers were dried with nitrogen gas. The oxygen plasma treatment (Power = 100 watts, time= 2mins, and pressure= 2 mbar) was done to these wafers. The surface of the wafers treated with 1% of 3-aminopropyltriethoxysilane (APTES) for 20 min. Then the wafers kept in the hot oven at 120^{o}C for 4 min. The gel sample dispensed on the wafers and left undisturbed for 5 min. After five minutes, the wafer was cleaned thoroughly with water. Then the wafers were kept in the desiccator for drying for 24 hours. The dried substrates were used for further analysis.

Atomic force microscopy:

Bruker Multimode 8.0 was used for the topographic imaging of the nanosheets, which is then used to find the thickness through Nanoscope analysis software. Silicon wafers of 1 cm × 1 cm were taken for analysis. These wafers were then cleaned with water, acetone, ethanol, isopropanol, and again with acetone. Each time, these wafers were dried with nitrogen gas. The oxygen plasma treatment (Power = 100 watts, time= 2mins, and pressure= 2 mbar) was done on these wafers. The surface of the wafers treated was with 1% of 3-aminopropyltriethoxysilane (APTES) in ethanol solution for 20 min. Then the wafers were kept in the hot air oven at 120^{o}C for 4 min. Then the gel sample was dispensed on the wafers and left undisturbed for five min. After five minutes, the wafer was cleaned thoroughly with water. Then the wafers were kept in the desiccator for drying for 24 hours. The dried substrates were used for further analysis.

3.4.2 Optical characterization:

Raman Analysis:

HR800-UV confocal micro-Raman spectrometer with 532 nm laser source was used for the analysis. Typically, 5 mg of lyophilized nanosheet powder and pristine TiB_2 powder were used and to focus the laser source on the samples, 10X objective lens was used. The scanning was done in the range of 100- 1200 cm^{-1} with a counting time of 30 s.

3.4.3 Macroscopic characterization:

TG-DSC Analysis:

Thermogravimetric and differential scanning calorimetric analysis (TG-DSC) was performed on a TG-DSC instrument (NETZSCH, STA 449 F3 Jupiter). TG experiments were conducted under a nitrogen environment. The flow rate was maintained at 20 cm^3 min^{-1}, and the heating rate was 10^oC min^{-1}.

3.5 Results and discussion:

Optical microscopy analysis:

We have seen the large sheets from the FESEM. From the optical microscope, also we saw large sheets, which have the lateral dimensions even greater than 100 µm. It is also observed that some sheets are nicely folded, which can be seen from the figure 3.11 (a, f, i), some are torn apart (figure 3.11 (d, h)), some are bent (figure 3.11(e)), and some have nice branching or flower structure (figure 3.11(g)).

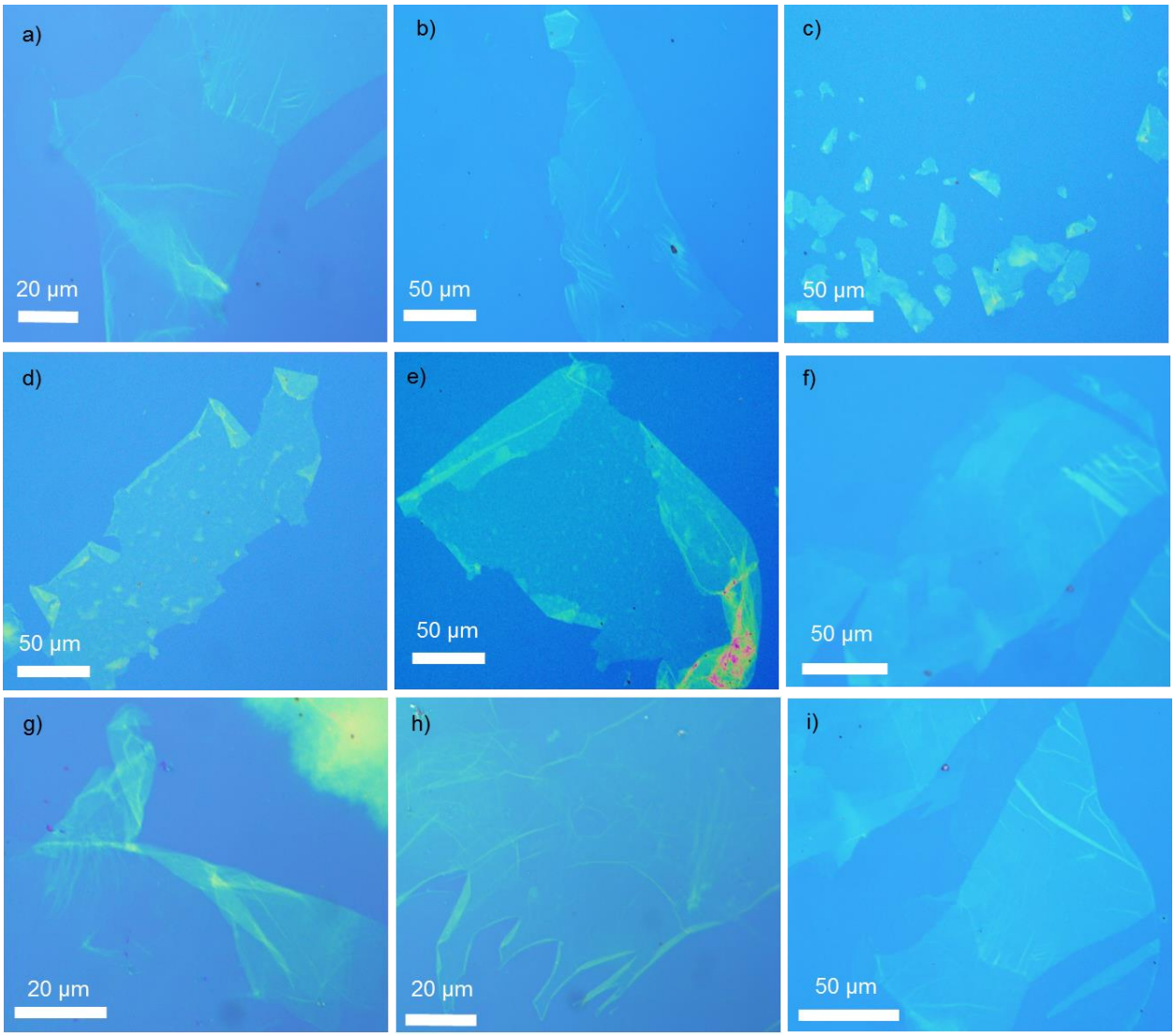

Figure 3. 11 Optical microscopy images of the gel after one day of post-dialysis. (a, b, f, and i) indicating the larger sheets along with some portion are nicely folded; (d, and h) showing the edges are torn apart; (e) showing the bending in the edges; (c) so many small nanosheets; (g) showing the branching like the structure of nanosheet;

AFM Analysis:

The optical images were used as a reference while doing AFM analysis to exactly place the cantilever tip on the large sheets to see the topography and the thickness of the sheets. As the sheets were very large, so we had to do a large area scan to see the sheets. The scan was done at an area of 50 µm × 50 µm. Figure 3.12 (a, b) shows some part of the nanosheets, whereas figure 3.12 (a', b') shows the thickness plot of these sheets. The thickness measurement has

done between the two highlighted points on the figures, and it is found to be around 4 nm in both cases.

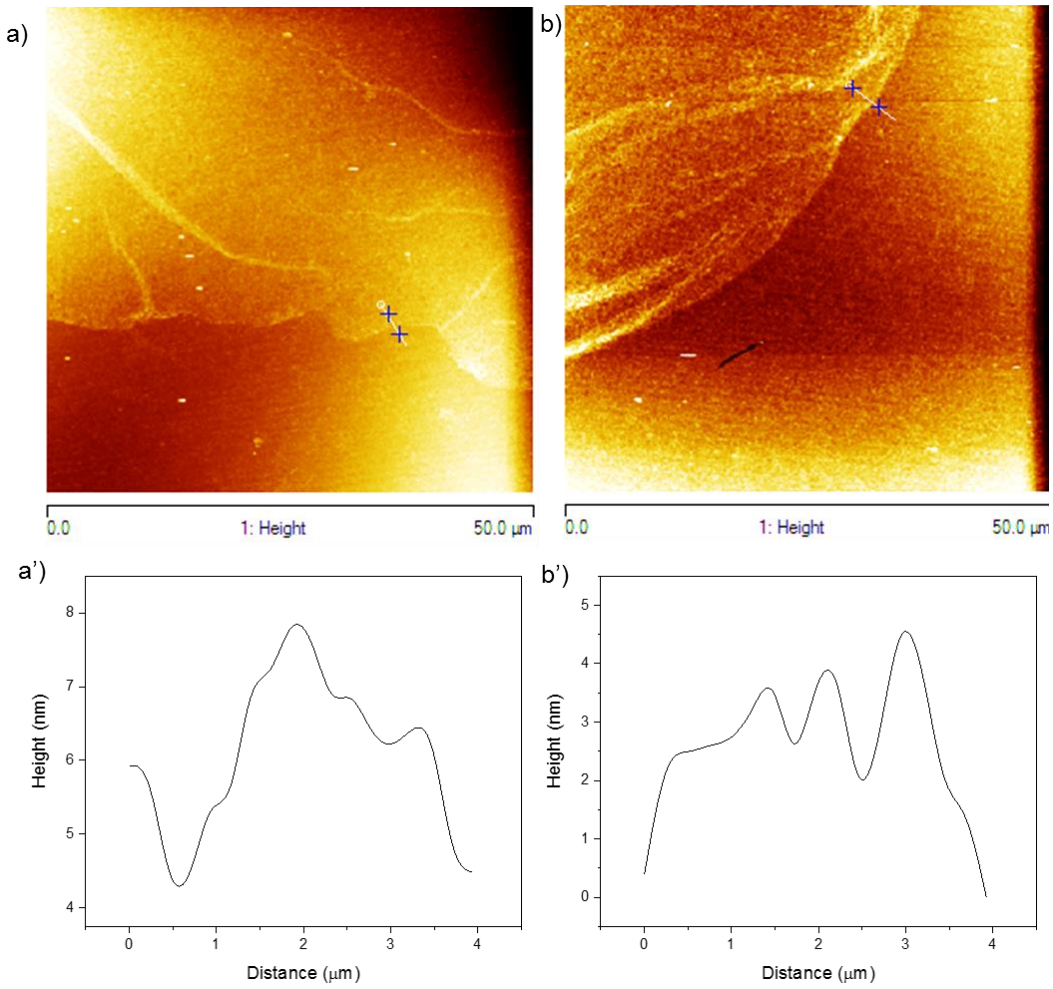

Figure 3. 12 AFM images of the gel after one day of post-dialysis. (a, b) Showing the topography of the nanosheets and (a', b') indicating the thickness plot of these images. The thickness of the nanosheets is around 4 nm in both images.

Raman Analysis:

The Raman spectrum of the pristine TiB_2 shows four peaks at 143 cm^{-1}, 250 cm^{-1}, 420 cm^{-1}, and 610 $cm^{-1,}$ which agrees reasonably well with the observations made by Urszula et al. at the same excitation wavelength that is 532 nm.[55] The Raman active E_{2g} mode is found to be at 610 cm^{-1} in the pristine TiB_2, which corroborates the presence of B-B in-plane stretching mode. While the nanosheets showing the peaks at 285 cm^{-1}, 525 cm^{-1}, 700 cm^{-1}, and 905 cm^{-1}. The

peaks that the nanosheets exhibit are very similar to the pristine TiB_2, but a little shift in the peaks is there. Thus we can say that the peak 700 cm^{-1} corresponds to the E_{2g} mode of the nanosheets. The shift in the E_{2g} mode may be due to two reasons. The first one is a reduction in thickness (Yang et al. observed that reducing the thickness of the TiO_2 nanosheets results in the shift of the E_{2g} mode peaks to the right side[56]). The second reason is the presence of functional groups (Georgakilas et al. and Haubner et al. observed that the presence of functional groups in the graphene results in the shifting of the peak of the G band/E_{2g} phonon[57,58]).

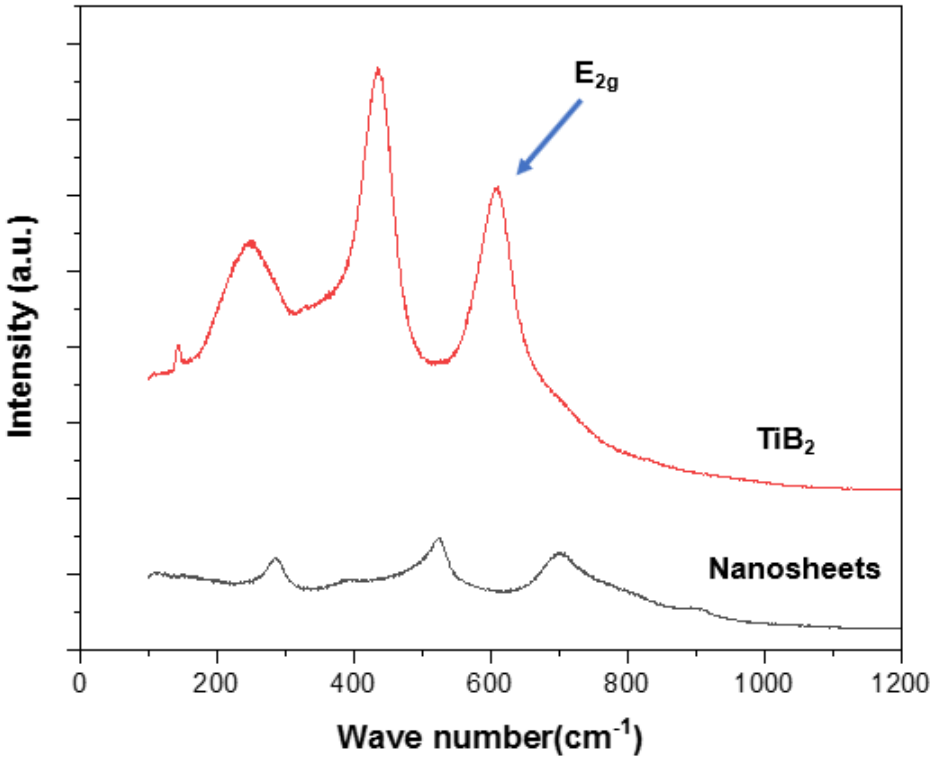

Figure 3. 13 Raman spectrum of pristine TiB_2 and nanosheets are showing the presence of E_{2g} mode. The E_{2g} mode suggests the presence of B-B honeycomb planes.

TG-DSC Analysis:

It is found from the thermogravimetric analysis (TGA) that titanium diboride nanostructures exhibit a mass loss of around 27 % at a temperature range of 30-450°C. This mass loss may be due to the removal of moisture present and oxygen-containing functional groups. Similarly, It has been observed that graphene oxide exhibits mass loss up to 300°C, which is due to the removal of oxygen-containing functional groups.[59] From the differential scanning calorimetric

(DSC) analysis, it is analyzed that there are no peaks observed when the sample is heated up to 1200 ^{o}C. This means that there is no melting, crystallization, or phase transition is happening. This indicates that titanium diboride based nanostructure is highly thermally stable. But graphene gets burned up at a temperature of 584^{o}C, which is low as compared to our material.[60]

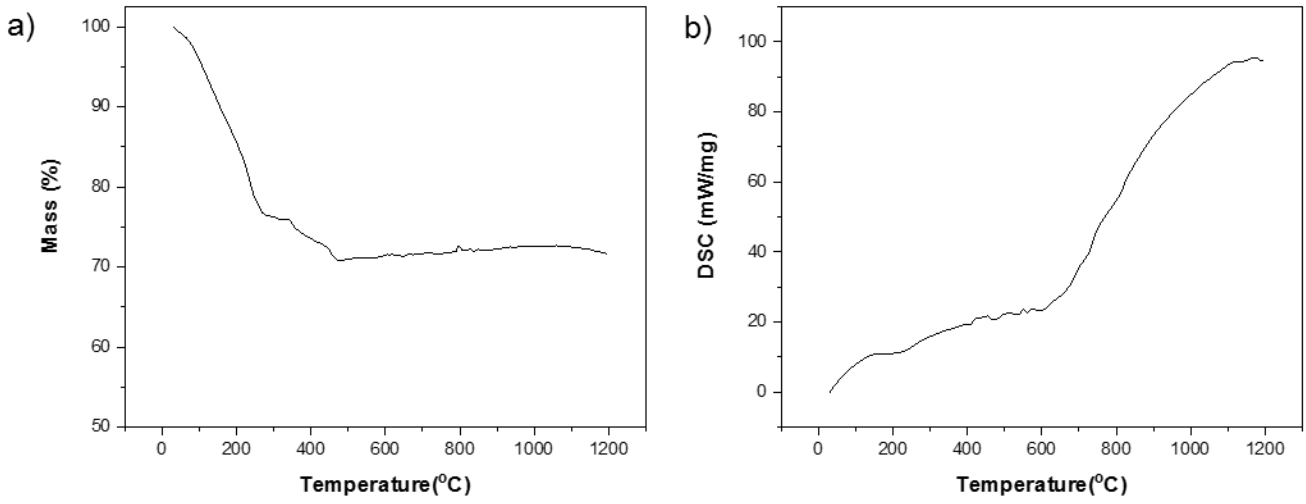

Figure 3. 14 (a) TGA curve indicating the mass loss up to 450^{o}C; (b) DSC curve shows nanostructures are highly thermally stable.

3.6 Conclusion:

Time-dependent analysis through TEM suggests the mechanism of larger sheet formation. It gives us an idea of the bottom-up approach synthesis of nanosheets. It was found that the titanium diboride is undergoing dissolution, which is then followed by non-classical crystallization to get the large sheets. In addition, it is found that the growth is in the lateral dimension only, which was found from the AFM analysis. On the other hand, through Zeta potential analysis, it was confirmed that the electrostatic forces of attraction are not responsible for the gel formation. Then a reduction process proved that the gel formation is mainly due to the chemical crosslinking. The chemical crosslinking is found to be borate crosslinking from the FTIR analysis. Optical microscopy and atomic force microscopy shows the presence of very large sheets. While Raman spectroscopy confirms the presence of B-B in-plane stretching tells that these nanosheets are comprised of honeycomb planes of boron. From the

TG analysis of our sample, it was found that the loss of 27 % up to temperature 450^{o}C indicates the loss of oxy functional groups. In addition, DSC shows that titanium diboride based nanostructure are thermally stable in nature. Furthermore, we have found the rheological properties of the gel, which is presented in the next chapter.

Chapter 4: Rheology of boron-based hydrogel

4.1 Introduction:

After finding the mechanism for the gel formation, we moved on to analyze the properties of the boron-based hydrogel. Here, we discuss rheological properties like storage and loss modulus, which were found through different experiments. These experiments were carried out by varying the parameters like concentration of the reactants and time. Then we compare these results and find the concentration of reactants at which gel has a higher storage modulus. In addition, we discuss the relationship between the gel strength (elastic part of the gel) and the morphology of the dispersed phases in the gel.

4.2 Rheological characterization:

The rheological properties of the hydrogels were measured using Anton Paar, Modular Compact Rheometer having model number MCR 302 with the stress and strain controlled. The measurements have been taken at a constant temperature of 25^0C with a cone-plate geometry (CP25) having 25mm diameter and 2^0 truncation angle. A constant gap of 0.105 mm was maintained between the geometry and the platform. In addition, a solvent trap was used to avoid solvent evaporation. The following measurements were performed to understand the rheological properties of the gel.

(a) Small amplitude oscillatory frequency sweep measurements were performed to study the viscoelastic behavior of the boron-based hydrogel. The samples were subjected to the angular frequency (ω) of 100-0.1 rad/s and an oscillatory strain (γ) of 0.5%. These conditions ensured that the storage and loss modulus were measured in the linear viscoelastic region.

(b) Large amplitude oscillatory strain sweep measurements were carried out to study the nonlinear response of the boron-based hydrogel in the range of an oscillatory strain (γ) of 0.01-1200% at a constant angular frequency (ω) of 6.28 rad/s.

(c) Time sweep measurements were executed to study the time-dependent behavior of the boron-based gel. All the data points have been measured at an interval of 1 minute by

keeping the oscillatory strain and angular frequency at a constant value of 0.5% and 6.28 rad/s respectively.

Frequency sweep, amplitude sweep, and time sweep measurements of all the samples (boron-based hydrogel) which were prepared by adding TiB_2/H_2O_2 as 30, 60, 90, 150, & 180 were taken. The measurements of these samples were carried out at 0^{th}, 1^{st}, 2^{nd}, 4^{th}, 6^{th}, and 8^{th} day. Each day's samples were stored separately in a closed plastic container at room temperature, and the aluminum foil was wrapped around the container.

4.3 Results and discussion:

4.3.1 Rheological analysis:

Frequency sweep Analysis:

Figure 4.1 shows the small amplitude oscillatory frequency sweep measurements of different samples in which (a, b, c, d, & e) represent the samples, which were prepared by taking TiB_2/H_2O_2 as 180, 150, 90, 60, & 30 respectively. For all the samples, each day shows a higher value of storage modulus as compared to the loss modulus (G´> G´´). Even we can say that all the samples are becoming hydrogels after just the completion of processing, i.e., from the 0^{th} day onwards. It is noticed that both the moduli remain constant in the frequency range of 0-60 rad/s in all the samples. Also, it is observed that throughout the entire range of tested frequency (0.1-100 rad/s), no crossover occurs in the samples (except TiB_2/H_2O_2=30 sample). Whereas the boron-based gel having TiB_2/H_2O_2=30 shows the cross overs at a higher frequency (> 50 rad/s). Crossover at higher frequency means the relaxation time is low, which suggest that this sample shows liquid-like behavior.

It is found out that the boron-based hydrogel with high and low TiB_2/H_2O_2 does not give a high value of storage modulus even after eight days, as the value is coming to around 50 Pa in the samples having TiB_2/H_2O_2 as 180 and 30. But it is observed that the samples having TiB_2/H_2O_2=90 gives a G´ of 350 Pa which is quite higher than the other samples. Also, these samples do not have any cross over in the tested frequency range.

The boron-based hydrogels have a chemical crosslinking network, which is mainly by the borate groups (described in chapter 3). When the cross over is occurring in our hydrogel, that means the gel is converting to the liquid by breaking the chemical crosslinking. The cross over is observed in the samples having TiB_2/H_2O_2=30 at a high frequency (>50 rad/s). This indicates that the chemical crosslinking is breaking at a frequency of 50 rad/s in the sample having TiB_2/H_2O_2=30. We can also say that the chemical crosslinking is very strong in the sample having TiB_2/H_2O_2=90 for which we are getting a G´ of 350 after the 8th day.

Murata et al. have reported that when the critical gelation concentration (CGC where a sol-gel transition occurs) is below one wt.%, then the gel can be called as supergelator.[61] In our studies, the concentration of the nanoparticles in the boron-based gel is coming around 3 mg/ml (0.3 wt.%), and its CGC must be lower than 0.3 wt.%. Thus, we can say our boron-based gel as a supergelator. The spuergelator also has been reported in the graphene oxide gel through ultrasonication by Owen et al.[53]

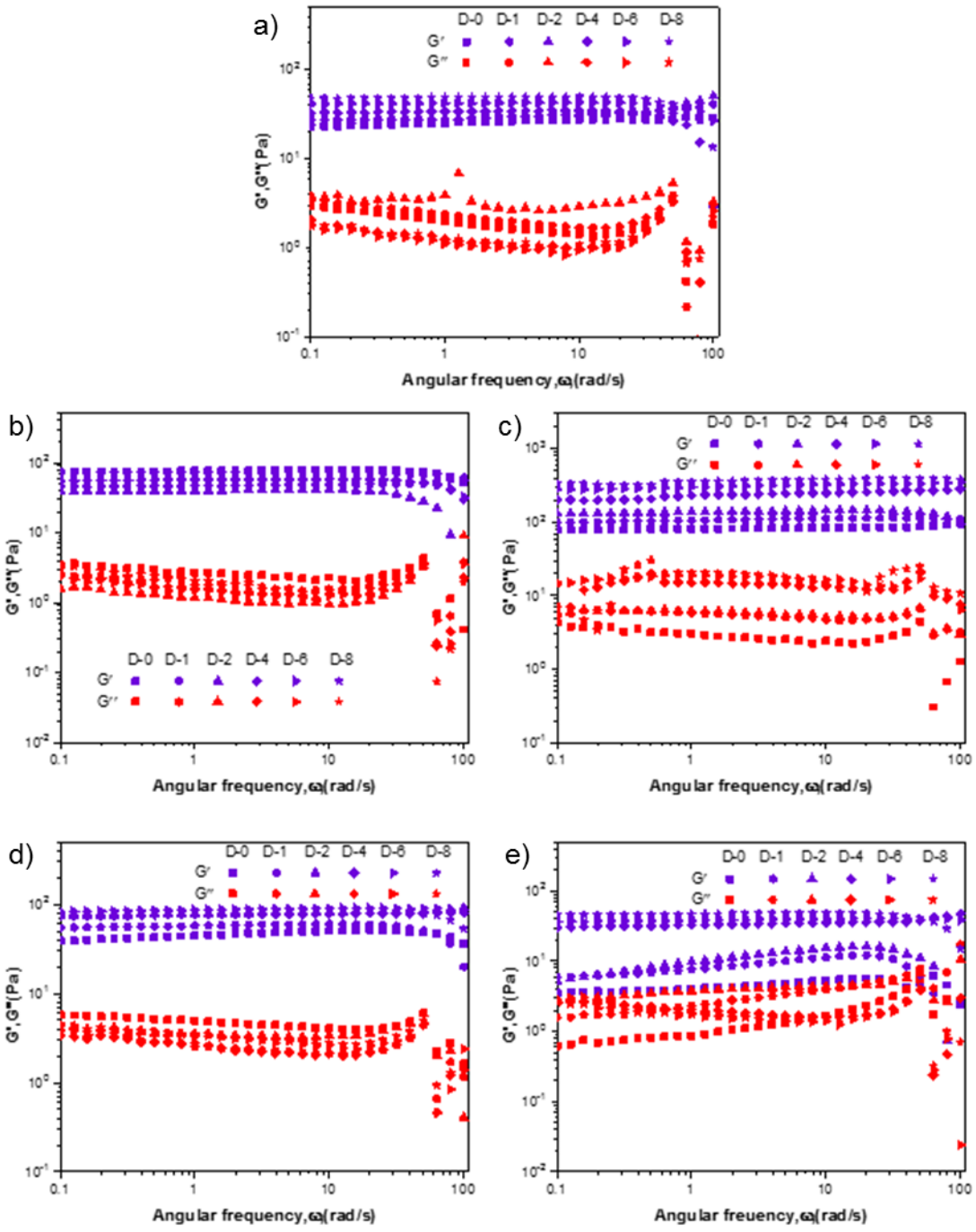

Figure 4. 1 Small amplitude oscillatory frequency sweep measurements of different samples in which (a, b, c, d, & e) represent the samples which were prepared by taking TiB_2/H_2O_2 as 180, 150, 90, 60, & 30 respectively. In all case the G´ > G´´ and there is a consistency in both value of G´ and G´´ up to an angular frequency of 50 rad/s. (c) no changes in the G´ at the tested frequency range. (e) Crossover is happening at a higher angular frequency.

Amplitude sweep Analysis:

The figure 4.2 shows the large amplitude oscillatory strain sweep measurements of different samples in which (a, b, c, d, & e) represent the samples which were prepared by taking TiB_2/H_2O_2 as 180, 150, 90, 60, & 30 respectively. It is found that all the boron-based hydrogels show G´> G´´, with both the moduli being independent of applied strain (γ) to 1%. But we can see that the sample, which is prepared with TiB_2/H_2O_2= 90 shows higher stability with the increase of applied strain and both moduli remain constant up to 3% applied strain (figure 4.2(c)). Thus the yielding of the hydrogels of the samples having TiB_2/H_2O_2= 90 starts at a higher strain (3 %) as compared to the other samples (~1%). In all the samples, the crossover of G´ and G´´ is there within the tested applied strain (0.01- 1200 %). After crossover the G´´> G´ which indicate that the gel converts to liquid by breaking the chemical crosslinking networks. The strain at which the cross over occurs depends on the time in days and the ratio of TiB_2/H_2O_2 which was used for the preparation of the boron-based hydrogels.

In addition, we can see that the values of both storage and loss modulus in amplitude sweep in the linear viscoelastic region are consistent with the frequency sweep experiments.

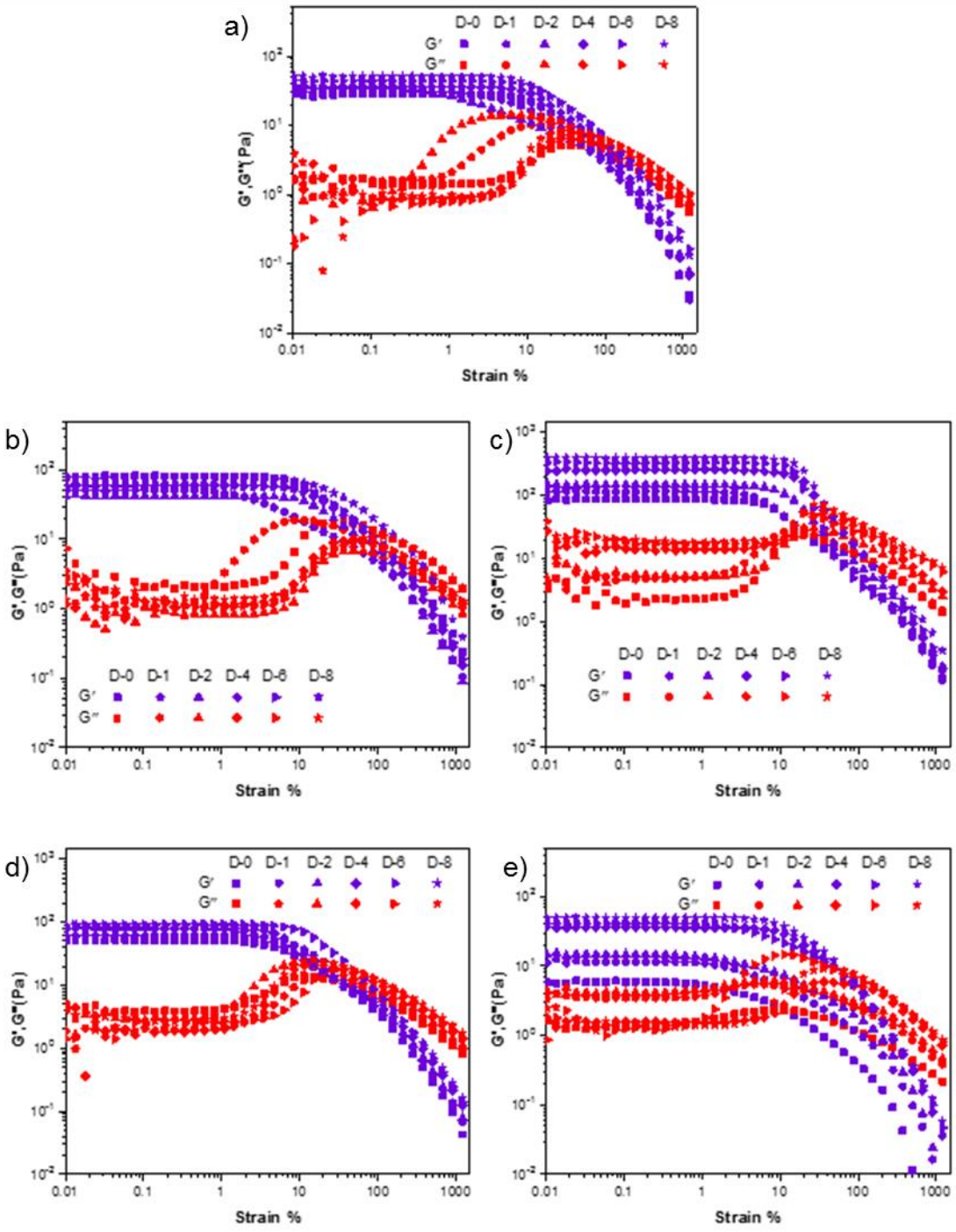

Figure 4. 2 Large amplitude oscillatory strain sweep measurements of different samples in which (a, b, c, d, & e) represent the samples which were prepared by taking TiB2/H2O2 as 180, 150, 90, 60, & 30 respectively. In all the samples G´ > G´´ and these values are consistent with the frequency sweep experiments. In a, b, d, & e show the decrease in the G´ starts at ~1% while in case of c the stability

maintained up to 3% applied strain. In each case, there is a crossover, suggesting the breaking of chemical crosslinking.

Time Sweep Analysis:

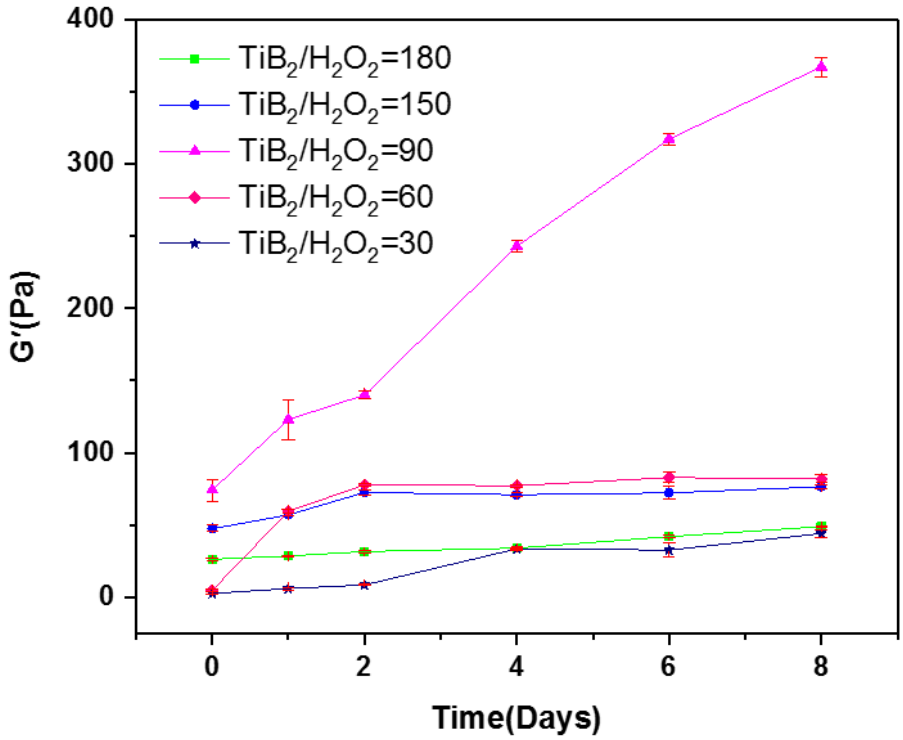

Figure 4. 3 Average G' variation in days shows the hydrogel which was prepared by taking TiB_2/H_2O_2 as 90 has a very high storage modulus values as compared to others. Also, this sample shows a higher increment in the G´ as compared to other samples.

Figure 4.3 shows the plot of average storage modulus (G'_p) alteration with days. The G'_p values are deduced from the time sweep experiments, which were conducted for 20 minutes on different days. For each hydrogel, two runs have been taken, and from that, the error bars have been calculated, which is shown in figure 4.3. The error bars are very small, indicating the consistency in the storage modulus values at different trial. The boron-based hydrogel, which was prepared with the TiB_2/H_2O_2 of 90, has an excellent storage modulus and it increases from 60 Pa in 0^{th} day to 350 Pa in the 8^{th} day and it does not reach saturation in a period of 8 days whereas other samples show less storage modulus (< 100 Pa) and also reach saturation within 8 days.

4.3.2 Morphology studies of the hydrogels with time:

The sample with TiB_2/H_2O_2 ratio of 180 subjected to lyophilization at different days. We obtain a light yellowish white color powder. These powders were then analyzed under FESEM to know the morphology factor in the gel formation. Figure 4.3 shows that morphology of the dispersed phases of the gel at different days. Figure 4.3 (a) represents the morphology of the gel after the 0^{th} day, which shows the presence of both nanosheets and nanowools. Similarly, both nanosheets and nanowools can be found in the gels at different days. However, something we observed that the nanowools that are forming, getting deposited on the nanosheets by aggregating with each other or isolated. This kind of deposition creates crumples on the nanosheets, which can be seen from the figure 4.3 (b, c, f) where b & c represents the gel morphology after two days, and f represents the morphology of the gel after six days. Also, the deposition of the nanowools is evident from the figure 4.3 (e, h, i) where e, h, and I represents the morphology of the gel after four days, six days, and eight days respectively. We can conclude that there is the presence of both nanosheets and nanowools along with this the aggregation of nanowools is also happening, which result in crumpledness on the nanosheets. All this process is occurring on every day. This suggests that morphology of the sheets is not playing a significant role in gel formation. Also, we have described that chemical crosslinking helps in gel formation.

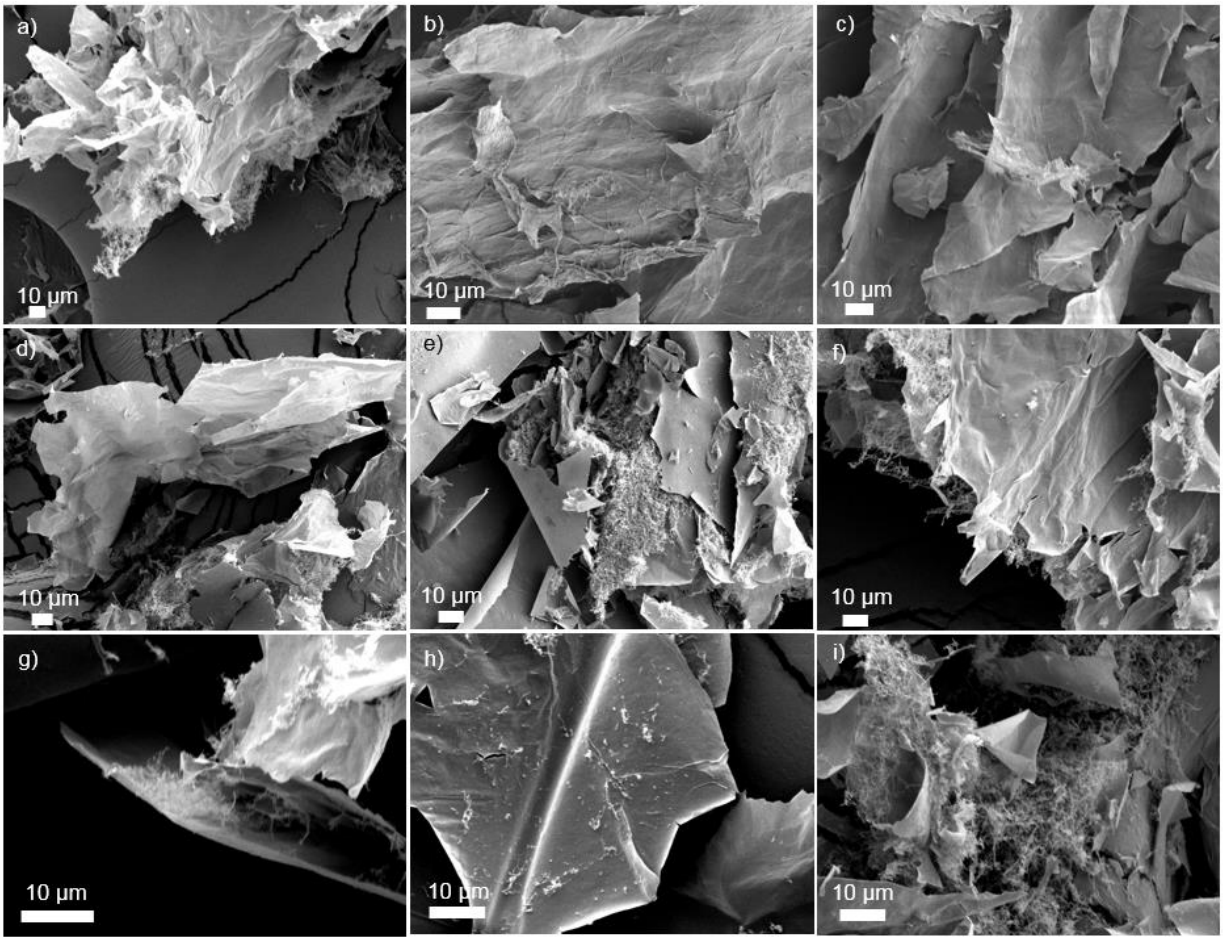

Figure 4. 4 morphology of the dispersed phases of the boron-based gel at different days, which was prepared by taking TiB_2/H_2O_2=180. (a) 0th day: showing the presence of both nanosheets and nanowools. (b, c) 2nd day: shows the presence of both sheets and wools along with wools has been deposited in the sheets. (d, e) 4th day: shows the presence of both nanosheets and nanowools along with aggregation of nanowools in some place. (f, g, h) 6th day: all the above things can be seen. (i) 8th day: shows the presence of both nanosheets and nanowools.

4.5 Conclusion:

It is found out that the G´ > G´´ in each sample at various days, which shows the gel-like behavior. However, in the frequency sweep experiments, a sample having TiB_2/H_2O_2 30 indicates a crossover at higher frequencies suggesting liquid-like behavior. The rate of increase of storage modulus value is very high in case of gel having TiB_2/H_2O_2=90 w.r.t days. Here, it

increases from the 60 Pa in 0^{th} day to 350 Pa in the 8^{th} day. While other samples remain below 100 Pa on different days with the increase of G´ very slow, which indicates samples are stabilizing. In addition, it is found from the morphology studies of the dispersed phase of the gel that there is no correlation between the structures of the nanosheets, which again confirms that the gel is forming due to the chemical crosslinking only.

Chapter 5: Conclusion and Future works

5.1 Conclusion:

This thesis began with an unexpected observation of gel formation with a simple mixing of titanium diboride with hydrogen peroxide and water. The resultant mixture turns yellow color with time, which resulted in the gelation after five days. Here, we optimized the parameters like mixing time and reactant concentration to get a hydrogel in just one day only. Tyndall beam effect indicated the presence of dispersed particles. The dispersed phase is found to be nanosheets from the FESEM analysis, and the sheets have lateral dimensions greater than the size of the parent titanium diboride crystals. It is also observed through FESEM that some nanowools aggregate on the sheets. FTIR spectrum revealed the presence of oxy functional groups.

We also presented our understanding of the possible mechanism behind the large sheets and gel formation. The non-classical crystallization is occurring in our system, which is found from the TEM analysis. The formation of pre-nucleation clusters (PNCs) happens due to the dissolution of titanium diboride crystals, which then self-assemble/aggregate to form large sheets. The aggregation is mainly occurring in the lateral dimension, which is found from the AFM analysis. The reduction of the gel with ascorbic acid proved that gel is forming due to the chemical crosslinking. The chemical crosslinking is found to be mainly due to borate groups, which are found from the FTIR analysis.

In addition, we observed the large sheets through optical microscopy and AFM. Raman analysis indicates the presence of boron honeycomb planes in the nanosheets. The nanosheets are found to be thermally stable from TG-DSC analysis.

All the ratio of the reactants resulted in the gel formation. However, the boron-based hydrogel, which was prepared from TiB_2/H_2O_2 of 90 has a very high storage modulus. The rate of increase in the storage modulus values is also found to be high in this sample only. In other samples, the rate is very slow, suggesting the stabilization of gel is happening. It is found from the FESEM images that there is the presence of nanosheets and nanowools in the samples at different days, which suggest that morphology doesn't play a significant role in the gel formation. It is the chemical crosslinking which plays a key role in the hydrogelation.

5.2 Future work:

In the present work, we demonstrated the formation of a hydrogel, when TiB_2 interacted with H_2O_2/H_2O solvent mixture and found that chemical crosslinking is the reason for the formation of this hydrogel. The rheological studies revealed that the storage modulus is very high only at a particular concentration ratio of TiB_2/H_2O_2. Therefore, it would be very much interesting to find the answer to the question: why the storage modulus value is very high at a particular concentration ratio of TiB_2/H_2O_2 and with moving up or down from that concentration ratio, why the storage modulus value decreases.

As the sheets have very high thermal stability so, it would be great if we can prepare anything out of it like a composite material, which can be used in the space industry for its lightweight property.

The presence of nanosheets along with the nano-wool are looking like pores in our nanostructures obtain from titanium diboride. This can be used as a filter medium to filter out the smallest particle in the air. It would be great to develop an air filter, which will have high permeability of air and high efficiency in removing the PM2.5 particles. Researchers have been trying to get the porous structure in graphene by adding pulp, but in our case, it is already available.[62] As our materials already have nanowools, which can be used as the pores to prevent PM2.5 particles. Thus the presence of nanowools creates an upper hand to our material, which can be used as an air filter.

Generally, the hydrogels are highly porous. So, it can be used for drug delivery into a specific location in our body. Due to the porous structure of the hydrogel, drugs can be easily inserted. In addition, we can easily tune the properties, i.e., storage and loss modulus values of the boron-based hydrogels (we have done here by changing the concentration of TiB_2/H_2O_2) to disintegrates the hydrogel in the specific location of the body so that drugs can be placed on that particular location only.

Bibliography

1. Hobson, D. W. Nanotechnology. in *Comprehensive Biotechnology, Second Edition* (2011). doi:10.1016/B978-0-08-088504-9.00228-2

2. World's Smallest Motor: The McLellan Micromotor • Pasadena Museum of History. Available at: https://pasadenahistory.org/collections/micromotor/. (Accessed: 20th June 2019)

3. Tiwari, J. N., Tiwari, R. N. & Kim, K. S. Zero-dimensional, one-dimensional, two-dimensional and three-dimensional nanostructured materials for advanced electrochemical energy devices. *Progress in Materials Science* (2012). doi:10.1016/j.pmatsci.2011.08.003

4. Onoue, S., He, J. & Kunitake, T. Fabrication of Gold Nanosheet and Nanowire by Oxygen Plasma Induced Fusion of Densely Arrayed Nanoparticles. *Chem. Lett.* (2006). doi:10.1246/cl.2006.214

5. Iacopi, F. (Francesca), Boeckl, J. J. & Jagadish, C. (Chennupati). *2D Materials*.

6. Novoselov, K. S. *et al.* Electric field effect in atomically thin carbon films. *Science* **306**, 666–9 (2004).

7. Wang, H. *et al.* MoSe2 and WSe2 nanofilms with vertically aligned molecular layers on curved and rough surfaces. *Nano Lett.* (2013). doi:10.1021/nl401944f

8. Shahil, K. M. F., Hossain, M. Z., Teweldebrhan, D. & Balandin, A. A. Crystal symmetry breaking in few-quintuple Bi2 Te3 films: Applications in nanometrology of topological insulators. *Appl. Phys. Lett.* (2010). doi:10.1063/1.3396190

9. Goli, P., Khan, J., Wickramaratne, D., Lake, R. K. & Balandin, A. A. Charge density waves in exfoliated films of van der waals materials: Evolution of raman spectrum in TiSe2. *Nano Lett.* (2012). doi:10.1021/nl303365x

10. Novoselov, K. S. *et al.* Two-dimensional atomic crystals. *Proc. Natl. Acad. Sci. U. S. A.* **102**, 10451–3 (2005).

11. Coleman, J. N. *et al.* Two-dimensional nanosheets produced by liquid exfoliation of layered materials. *Science (80-.).* **331**, 568–71 (2011).

12. Liu, L. *et al.* Solid Exfoliation of Hexagonal Boron Nitride Crystals for the Synthesis of Few-layer Boron Nitride Nanosheets. *Chem. Lett.* (2013). doi:10.1246/cl.130562

13. Kong, D. *et al.* Few-layer nanoplates of Bi2Se3 and Bi 2Te3 with highly tunable chemical potential. *Nano Lett.* (2010). doi:10.1021/nl101260j

14. Liu, D. *et al.* Electronic origin of high-temperature superconductivity in single-layer FeSe superconductor. *Nat. Commun.* (2012). doi:10.1038/ncomms1946

15. Bianco, E. *et al.* Stability and Exfoliation of Germanane: A Germanium Graphane Analogue. *ACS Nano* **7**, 4414–4421 (2013).

16. Nakano, H. *et al.* Soft Synthesis of Single-Crystal Silicon Monolayer Sheets. *Angew. Chemie Int. Ed.* **45**, 6303–6306 (2006).

17. Zhang, L. *et al.* Nanoparticles in Medicine: Therapeutic Applications and Developments. *Clin. Pharmacol. Ther.* **83**, 761–769 (2008).

18. Penn, S. G., He, L. & Natan, M. J. Nanoparticles for bioanalysis. *Curr. Opin. Chem. Biol.* **7**, 609–615 (2003).

19. Gatoo, M. A. *et al.* Physicochemical properties of nanomaterials: implication in associated toxic manifestations. *Biomed Res. Int.* **2014**, 498420 (2014).

20. Deguchi, S., Alargova, R. G. & Tsujii, K. Stable dispersions of fullerenes, C60 and C70, in water. Preparation and characterization. *Langmuir* (2001). doi:10.1021/la010651o

21. Yamauchi, A. Gels: Introduction V. 1. *Gels Handb.* 4–12 (2001).

22. Mathur, A. M., Moorjani, S. K. & Scranton, A. B. Methods for Synthesis of Hydrogel Networks: A Review. *J. Macromol. Sci. Part C Polym. Rev.* (1996). doi:10.1080/15321799608015226

23. Dalwadi, C. & Patel, G. Application of nanohydrogels in drug delivery systems: recent patents review. *Recent Pat. Nanotechnol.* **9**, 17–25 (2015).

24. Ahmed, E. M. Hydrogel: Preparation, characterization, and applications: A review. *J. Adv. Res.* **6**, 105–121 (2015).

25. Hosmane, N. S. *Boron science : new technologies and applications*.

26. Norton, J. T., Blumenthal, H. & Sindeband, S. J. Structure of diborides of titanium, zirconium, columbium, tantalum and vanadium. *JOM* (1949). doi:10.1007/bf03398932

27. Vajeeston, P., Ravindran, P., Ravi, C. & Asokamani, R. Electronic structure, bonding, and ground-state properties of AlB2-type transition-metal diborides. *Phys. Rev. B - Condens. Matter Mater. Phys.* (2001). doi:10.1103/PhysRevB.63.045115

28. Das, S. K., Bedar, A., Kannan, A. & Jasuja, K. Aqueous dispersions of few-layer-thick chemically modified magnesium diboride nanosheets by ultrasonication assisted exfoliation. *Sci. Rep.* **5**, 1–11 (2015).

29. James, A. L. & Jasuja, K. Chelation assisted exfoliation of layered borides towards synthesizing boron based nanosheets. *RSC Adv.* **7**, 1905–1914 (2017).

30. Gunda, H., Das, S. K. & Jasuja, K. Simple, Green, and High-Yield Production of Boron-Based Nanostructures with Diverse Morphologies by Dissolution and Recrystallization of Layered Magnesium Diboride Crystals in Water. *ChemPhysChem* **19**, 880–891 (2018).

31. Das, S. K. & Jasuja, K. Chemical Exfoliation of Layered Magnesium Diboride To Yield Functionalized Nanosheets and Nanoaccordions for Potential Flame Retardant Applications. *ACS Appl. Nano Mater.* **1**, 1612–1622 (2018).

32. James, A. L., Khandelwal, S., Dutta, A. & Jasuja, K. Boron based nanosheets as reducing templates in aqueous solutions: towards novel nanohybrids with gold nanoparticles and graphene. *Nanoscale* **10**, 20514–20518 (2018).

33. Saraswat, R., James, A. L. & Jasuja, K. High yield synthesis of boron-based nanosheets. *Adv. Appl. Ceram.* **118**, 209–216 (2019).

34. Han, Y., Dai, Y., Shu, D., Wang, J. & Sun, B. Electronic and bonding properties of TiB2. *J. Alloys Compd.* **438**, 327–331 (2007).

35. Park, J.-H., Lee, Y.-H., Koh, Y.-H., Kim, H.-E. & Su Baek, S. Effect of Hot-Pressing Temperature on Densification and Mechanical Properties of Titanium Diboride with Silicon Nitride as a Sintering Aid. *J. Am. Ceram. Soc.* **83**, 1542–1544 (2010).

36. Tennery, V. J., Finch, C. B., Yust, C. S. & Clark, G. W. Structure-Property Correlations for TiB2-Based Ceramics Densified using Active Liquid Metals. in *Science of Hard Materials* 891–909 (Springer US, 1983). doi:10.1007/978-1-4684-4319-6_49

37. Bača, Ľ., Jogl, C., Neubauer, E., Vitkovič, M. & Merstallinger, A. Microstructure evolution and tribological properties of TiB2/Ni–Ta cermets. *J. Eur. Ceram. Soc.* **32**, 1941–1948 (2012).

38. Jain, A. *et al.* Determination of the thermodynamic stability of TiB2. *J. Alloys Compd.* **491**, 747–752 (2010).

39. Gu, M., Huang, C., Xiao, S. & Liu, H. Improvements in mechanical properties of TiB2 ceramics tool materials by the dispersion of Al2O3 particles. *Mater. Sci. Eng. A* **486**, 167–170 (2008).

40. John, S. K. & Anappara, A. A. Aqueous dispersions of highly luminescent boron-rich nanosheets by the exfoliation of polycrystalline titanium diboride. *New J. Chem.* (2019). doi:10.1039/C9NJ01502G

41. Titanium Diboride (TiB2) - Properties and Applications. Available at: https://www.azom.com/article.aspx?ArticleID=492. (Accessed: 11th June 2019)

42. About hydrogen peroxide. Available at: https://www.rsc.org/Education/Teachers/Resources/Contemporary/student/pop_peroxide.html. (Accessed: 11th June 2019)

43. Huang, F. *et al.* Effect of hydrogen peroxide on TiB<inf>2</inf>-based materials. *Adv. Mater. Res.* **66**, 222–225 (2009).

44. Caetano, B. L. *et al.* Mechanisms of SnO2 nanoparticles formation and growth in acid ethanol solution derived from SAXS and combined raman-XAS time-resolved studies. *Chem. Mater.* (2014). doi:10.1021/cm5032688

45. Banfield, J. F. Oriented attachment and growth, twinning, polytypism, and formation of metastable phases: Insights from nanocrystalline TiO2. *Am. Mineral.* (1998).

46. Penn, R. L. & Banfield, J. F. Imperfect oriented attachment: Dislocation generation in defect-free nanocrystals. *Science (80-.).* (1998). doi:10.1126/science.281.5379.969

47. Zhu, C. *et al.* In-situ liquid cell transmission electron microscopy investigation on oriented attachment of gold nanoparticles. *Nat. Commun.* (2018). doi:10.1038/s41467-018-02925-6

48. Ondry, J. C., Hauwiller, M. R. & Alivisatos, A. P. Dynamics and Removal Pathway of Edge Dislocations in Imperfectly Attached PbTe Nanocrystal Pairs: Toward Design Rules for Oriented Attachment. *ACS Nano* (2018). doi:10.1021/acsnano.8b00638

49. Schliehe, C. *et al.* Ultrathin PbS sheets by two-dimensional oriented attachment. *Science (80-.).* (2010). doi:10.1126/science.1188035

50. Gebauer, D. & Wolf, S. E. Designing Solid Materials from Their Solute State: A Shift in Paradigms toward a Holistic Approach in Functional Materials Chemistry. *Journal of the American Chemical Society* (2019). doi:10.1021/jacs.8b13231

51. Cölfen, H. & Gebauer, D. *Prenucleation clusters and non-classical nucleation*. *Nano Today* **6**, (2011).

52. Gebauer, D., Kellermeier, M., Gale, J. D., Bergström, L. & Cölfen, H. Pre-nucleation clusters as solute precursors in crystallisation. *Chem. Soc. Rev.* **43**, 2348–2371 (2014).

53. Compton, O. C. *et al.* Additive-free hydrogelation of graphene oxide by ultrasonication. *Carbon N. Y.* **50**, 3399–3406 (2012).

54. Li, D., Müller, M. B., Gilje, S., Kaner, R. B. & Wallace, G. G. Processable aqueous dispersions of graphene nanosheets. *Nat. Nanotechnol.* (2008).

doi:10.1038/nnano.2007.451

55. Wdowik, U. D., Twardowska, A. & Rajchel, B. Vibrational Spectroscopy of Binary Titanium Borides: First-Principles and Experimental Studies. *Adv. Condens. Matter Phys.* **2017**, 1–9 (2017).

56. Yang, X. H. *et al.* Ultra-thin anatase TiO 2 nanosheets dominated with {001} facets: thickness-controlled synthesis, growth mechanism and water-splitting properties †. doi:10.1039/c0ce00233j

57. Georgakilas, V. *et al.* Functionalization of Graphene: Covalent and Non-Covalent Approaches, Derivatives and Applications. *Chem. Rev.* **112**, 6156–6214 (2012).

58. Haubner, K. *et al.* The Route to Functional Graphene Oxide. *ChemPhysChem* **11**, 2131–2139 (2010).

59. Wojtoniszak, M., Zielinska, B., Kalenczuk, R. J. & Mijowska, E. Photocatalytic performance of titania nanospheres deposited on graphene in coumarin oxidation reaction. *Mater. Sci. Pol.* (2012). doi:10.2478/s13536-012-0008-1

60. Huang, H., Sun, G., Hu, J. & Jiao, T. Low Temperature Synthesis of MnO_2 /Graphene Nanocomposites for Supercapacitors. *J. Chem.* **2015**, 1–8 (2015).

61. Murata, K. *et al.* Thermal and Light Control of the Sol-Gel Phase Transition in Cholesterol-Based Organic Gels. Novel Helical Aggregation Modes As Detected by Circular Dichroism and Electron Microscopic Observation. *J. Am. Chem. Soc.* **116**, 6664–6676 (1994).

62. Xiong, X., Ji, N., Song, C. & Liu, Q. Preparation Functionalized Graphene Aerogels as Air Cleaner Filter. *Procedia Eng.* **121**, 957–960 (2015).